



Experimental investigation of machining of EN31 Steel in abrasive mixed rotary EDM with graphite and copper electrode

AJAY LAMBA^{1,*} and VIPIN²

¹Department of Mechanical and Automation Engineering, G. B. Pant Engineering College, Delhi, India

²Department of Mechanical Engineering, Delhi Technological University, Delhi, India
e-mail: ajaylamba22@gmail.com

MS received 19 May 2021; revised 28 January 2022; accepted 19 May 2022

Abstract. The present work proposes an integration of tool rotation and blending of silicon carbide powder with kerosene as dielectric fluid in electrical discharge machining of EN31 steel with graphite and copper electrode. Peak current, pulse on time and tool rotation were identified as the machining parameters to evaluate their effect on material removal rate, tool wear rate and surface roughness of EN31 steel. Full factorial experimentation was executed to study 3 factors at 3 levels. Surface morphology of workpiece and powder characteristics were studied and analysed with FESEM, EDS and XRD techniques. Furthermore, recast layer thickness and sub-surface microhardness of the workpiece were examined to evaluate micro-changes in the performance characteristics. The recast layer thickness achieved by the graphite electrode was 6.12 μm whereas, copper achieved a value of 32.29 μm in the proposed method. The proposed process enhanced the sub-surface microhardness from 514.59 HV0.5 to 533.23 HV0.5 with graphite electrode, and from 503.55 HV0.5 to 523.54 HV0.5 with copper electrode, respectively. Genetic algorithm was executed to perform multi-objective optimization.

Keywords. ANOVA; EDM; EN31 steel; non-conventional machining; optimization.

1. Introduction

Electrical discharge machining (EDM) is a worldwide established process employed for die and mould making. The process is suitable for machining of electrically conductive materials irrespective of its hardness. It is a contact-free, thermal erosion process of material removal between workpiece and tool electrode. The tool and workpiece are submerged in the dielectric fluid inside the working tank. The tool and workpiece are separated by a little gap (about 5–100 μm) [1] known as inter-electrode gap (IEG). With the help of DC pulse generator, the potential difference is applied which generates an electric field in the inter-electrode gap. As a result of the electric field and subsequent bombardment of electrons, sparking takes place leaving craters on the workpiece and tool surface. At this stage, a very high temperature of the order of 8,000°C – 20,000°C [2] results in the melting and vaporization of the interfaces. As a result, material ejection in the form of tiny particles, often known as debris, takes place. The operation of EDM is such that the workpiece remains stationary while the tool moves up and down continuously. This up and down movement of the tool has been precisely controlled by a servo controller which is an important part of the process

helping in the removal of debris. As the process is an intermittent sparking process, the upward movement of the tool occurs during the non-sparking time, often referred as pulse off time. During the pulse off time, sudden removal of shock wave generates a void, subsequently, filled by the surrounding dielectric fluid. In this small time frame, a little swirl generates which takes away all the debris from the inter-electrode gap. In this way, material removal takes place from the workpiece. The EDM process finds applications in automobile, tool making, aerospace and manufacturing industries. The process has many advantages like burr free operation, no mechanical stresses induced while machining, softer tool can machine hard workpiece and many others. Despite all these, it suffers from many disadvantages, out of which, the most focused one is its less machining rate. The other disadvantages include poor surface quality owing to micro-cracks and recast layer, difficulty in producing sharp corners due to tool wear, etc. In view of these challenges, the researchers across the globe have consistently tried for improvements in output performance measures i.e. material removal rate (MRR), tool wear rate (TWR) and surface roughness (SR) by taking optimal combinations of input process parameters. Furthermore, the researchers [3–8] have tried various modifications in set up, especially in past 2 decades, that resulted in powder mixed EDM (PMEDM), ultrasonic assisted

*For correspondence

EDM (UEDM), magnetic field assisted EDM (MFEDM), near dry EDM, rotating magnetic field and ultrasonic vibration assisted EDM, rotary EDM (REDM), etc. The two important and promising modifications namely rotary EDM (REDM) and PMEDM are further taken up for detailed analysis in this study.

Chow and Huang [9] conducted the electro discharge machining study with a modified disk electrode. The results stated that MRR reached maximum at around 10-20 rpm and decreased afterwards till 150 rpm. The tool rotation taken under study was 0, 10, 20, 50 and 150 rpm. The electrode wear was found to increase with increase in tool rotation. Wang and Yan [10] presented a study of drilling of $Al_2O_3/6061Al$ composite by using tool rotation in EDM. They claimed that rotating eccentric through-hole electrode produced higher MRR compared to solid electrode but electrode wear rate (EWR) recorded was also higher. They also mentioned that electrode polarity mostly affected MRR and SR while intensity of peak current affected EWR. Satsangi and Chattopadhyay [11] presented a study on machining parameters of a rotary EDM on steel with copper electrode. They found that MRR decreases with increase in tool rotation from 10 to 48 rpm. MRR remained highest on low tool rotation value. The SR was also found to increase with increase in tool rotation. Further, they concluded that high peak current with low tool rotation and pulse on time yielded high MRR and low peak current and tool rotation with high pulse on time yielded better surface finish. Dwivedi and Choudhury [12] conducted experiments on AISI D3 steel and found that the tool rotations have significantly improved the material removal rate and surface finish by 41% and 12%, respectively. They also identified that the final surface has less number of micro-cracks. Chattopadhyay *et al* [13] developed an empirical model in rotary EDM of EN-8 steel machined with copper electrode. The most significant parameters as revealed by results for MRR and TWR were pulse on time and peak current while for SR, tool rotation and peak current were the significant parameters. Further, the findings revealed that MRR and TWR reduced, while SR increased with an increase in tool rotation. Singh *et al* [14] presented a study of process parameters in argon gas assisted rotary EDM. The results revealed high electrode wear rate and surface roughness in rotary EDM (REDM) and air assisted EDM (AAEDM) compared to argon gas assisted EDM (AGAEDM). The MRR was found to be more in AAEDM than REDM and AGAEDM. Furthermore, the recast layer was found to be more in AAEDM compared to REDM and AGAEDM.

Kansal *et al* [15] presented an optimization of parameters in the PMEDM process and results indicated higher MRR and surface finish with silicon powder mixed dielectric fluid. Kansal *et al* [16] studied the effect of silicon powder mixing into the dielectric fluid on machining characteristics of AISI D2 die steel. The mixing of silicon powder in dielectric (4g/l) recorded higher MRR. Singh *et al* [17] studied the effect of adding graphite powder in dielectric

fluid on surface properties of superalloy Super Co 605. They found significant improvement in the surface finish of machined part from 2.23 to 1.99 μm . Kumar *et al* [18] compared the EDM and NPMEDM process by adding alumina nanopowder in dielectric fluid. The results showed higher MRR (from 32.75 to 47 mg/min) and better surface finish (from 2.245 to 1.487 μm) as compared to normal dielectric fluid.

According to literature review [9–14], the effect of tool rotation on MRR, TWR and SR is still very uncertain. It exhibited a lot of variation in output characteristics, like increased in one and decreased in another using different tool rotation ranges and work tool combinations. Furthermore, PMEDM study has shown improvements in MRR and SR [15–18]. An in-depth examination of these two domains revealed that the future potential of integrating these two research fields of EDM may open the door to improved machining practices in EDM industries. As a result, this research study attempted to investigate the blending of powder with dielectric fluid (i.e., kerosene) along with tool rotation to analyse the effect on MRR, TWR and SR when cutting EN31 steel using graphite and copper tools.

2. Experimental details

2.1 Work material

EN31 steel was taken as workpiece material. The chemical composition of the work material obtained via energy-dispersive X-ray spectroscopy (EDX) is given in table 1.

2.2 Experimental set up

A set up was developed to add tool rotation as the conventional EDM machine (Sparkonix 35A) does not have this facility. A servomotor was used to rotate the tool through chain and sprocket arrangement. As the process involves abrasive EDM, an auxiliary tank was fabricated for sparking the job. A stirrer was also used in the tank for proper mixing of silicon carbide powder with kerosene, base dielectric media. Out of different available options in powder type, silicon carbide powder was selected with focus on physical properties, availability and cost. These factors favours easy adaptability of the proposed change in EDM to industries. Silicon carbide powder exhibits high melting point (2975 °C) and electrical conductivity ($1 \times 10^7 \mu \Omega \bullet m$) which makes it suitable for the present work as

Table 1. The chemical composition (wt.%) of EN31 steel.

C	O	Si	P	S	Cr	Mn	Fe
5.16	1.57	0.26	0.05	0.11	1.55	0.64	90.65

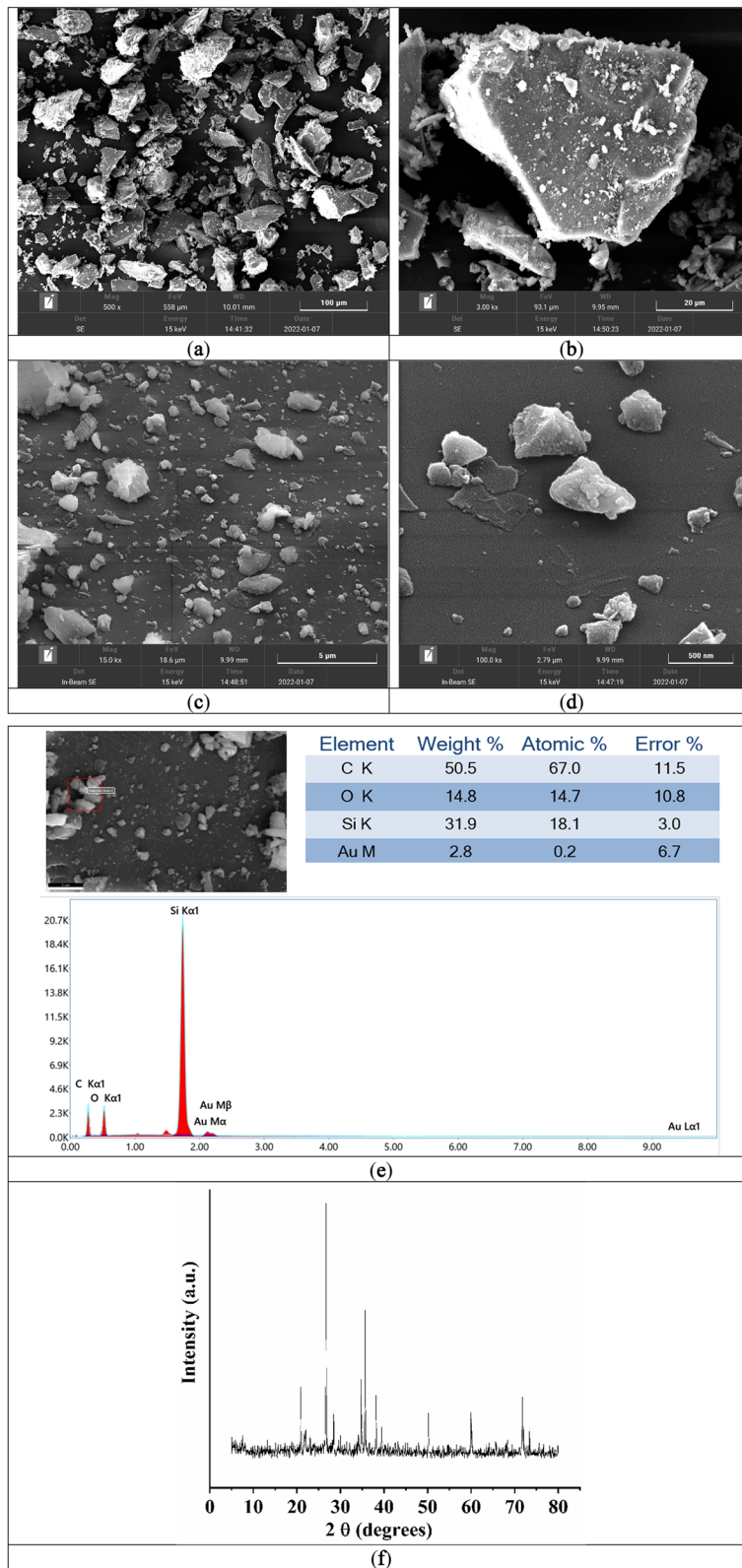


Figure 1. FESEM images of silicon carbide powder particles at (a) 500 x (b) 3 kx (c) 15 kx (d) 100 kx and (e) EDS of SiC; (f) XRD pattern of SiC.

it involves high current intensity and pulse on time leading to higher temperatures in machining. Furthermore, the researchers have presented results favouring this selection. Chow *et al* claimed that silicon carbide powder gained higher MRR compared with aluminium powder. Kung *et al* also highlighted the improvements in MRR, TWR and SR with silicon carbide powder. It is also stated that macro-sized silicon carbide powder was chosen over nano-sized powder because the larger the size of the powder, the greater the inter-electrode gap [19, 20]. Because this study proposes integrating tool rotation with PMEDM, the larger

gap, together with swirl impact of tool rotation to the dielectric, may result in improved surface integrity. Literature review of research in the micro range revealed that powder in the range of (10–50 μm) has shown improvements, yet the higher size has not been yet covered [21]. To fill the gap, a range of 60–100 μm was initially taken in trial experiments with powder sizes of 60, 80 and 100 μm . Out of these, initial results favoured the selection of 60 μm particle size. The size of the powder was calculated as 60 μm by Image J software based on recorded SEM images of ‘as received’ powder. Figure 1 depicts the relevant images.

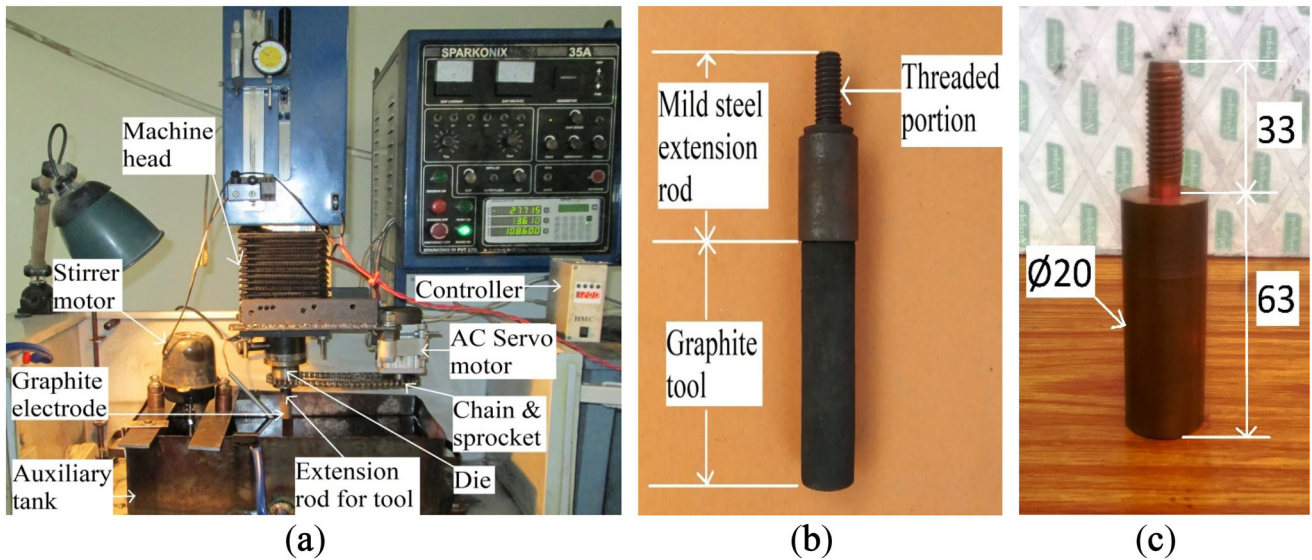


Figure 2. (a) Experimental setup; (b) graphite electrode; (c) copper electrode.

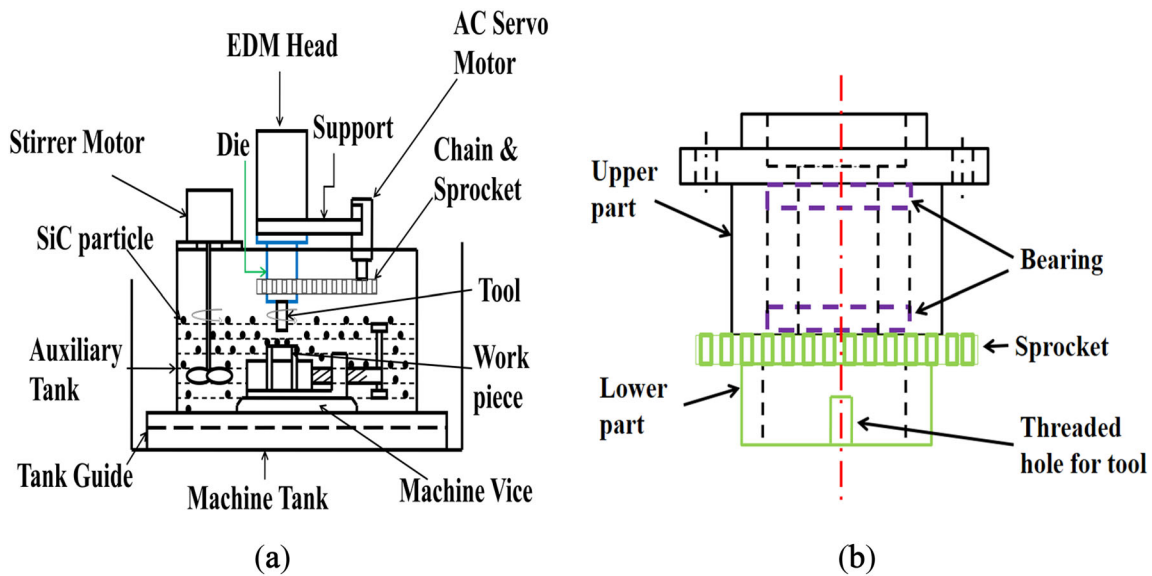


Figure 3. Schematics of (a) auxiliary tank; (b) die for tool rotation.

Table 2. Technical details of tool rotation set up.

Properties	Specifications
Motor type	AC Servo motor
Volts	220V
Output	550 W
Speed	100–5000 rpm

It can be elucidated from figures 1(a, b, c and d) that the size of powder particles was not homogenous. It varied from microns for larger particles to nano for smaller ones (refer figure 1(a)–(d)). As seen in figure 1(b), several smaller nano particles were discovered laying atop the larger ones. The variation of size can be better viewed from figures 1(c and d). Energy dispersive spectroscopy (EDS) and X-ray diffraction (XRD) of ‘as received powder’ are depicted in figures 1(e and f).

The rotational speed of stirrer shaft was measured by photo type digital tachometer (DT-2234B). The oil was not circulated during machining operation in different experimental runs. The experimental set up is shown in figure 2 (a), while figures 2(b and c) show the graphite and copper electrode. A schematic of experimental set up with auxiliary tank and die are also shown in figure 3 for detailed understanding. The technical details of tool rotation set up and experiments are mentioned in tables 2 and 3, respectively.

2.3 Selection of process parameters

The selection of process parameters is the most vital step in any research. The EDM researchers have explored many electrical and non-electrical parameters. The electrical parameters include pulse on time, pulse off time, peak current, servo voltage, etc. and non-electrical parameters include workpiece rotation, flushing of dielectric, tool rotation, electrode design. etc. In this research work, three process parameters, namely, peak current, pulse on time and tool rotation were selected based on literature survey and pilot experimentation. It was seen that most of the

Table 3. Technical details of experiments.

Properties	Unit	Specifications
Size of workpiece	mm × mm × mm	49 × 30 × 7.5
Size of tank	mm × mm × mm	510 × 285 × 160
Capacity of tank	litres	17
Powder type		Silicon carbide
Size of powder	microns	60
Concentration of powder	g/l	6
Stirrer	rpm	565

Table 4. Process parameters and their levels.

Process parameters	Symbol	Unit	Selected levels		
			I	II	III
Peak current	P_c	A	12	18	24
Pulse on time	T_{on}	μs	100	400	1000
Tool rotation	T_{rpm}	rpm	1200	1500	1800

research focused on low range of peak current, which can be used as finish cut. Now, as we know that EDM suffers from low MRR, so, machining with rough-cut becomes an open scope for research as exploring this area with supportive surface analysis including recast layer formation and sub-surface microhardness can reveal the intensity of peak current for finish cut as per the surface finish requirements of the workpiece. Considering this, it was further identified that published work in EDM has a research gap from mid to higher range of these selected parameters as most researchers have published work in the low range of peak current (1–10 A) [22, 23], pulse on time and tool rotation (up to 1000 rpm) [8–13]. It is also mentioned that level selection for pulse on time to 100, 400, 1000 μs was actually limited by the available panel options on EDM machine (Sparkonix 35A). Considering literature and machine constraints, rough cut machining in the range of 12–24 A for peak current, 100–1000 μs for pulse on time and 1200–1800 rpm for tool rotation was focused in this study. The selected parameters along with their unit, symbol and levels are shown in table 4.

2.4 Evaluation of response measures

The weight loss for calculation of material removal rate and tool wear rate were measured on Sartorius BSA 224S-CW weighing machine. The material removal rate (MRR) was measured as the ratio of the difference of the initial and final weight of the workpiece to total time of machining [24]. The values were recorded in mg/min. The MRR was calculated as $MRR = \frac{(W_i - W_f)}{T_m}$; where, W_i and W_f signify the initial and final weights of the workpiece in mg, respectively, and T_m is the total machining time in minutes. The tool wear rate was also measured as the ratio of difference of initial and final weight of tool to total time of machining in mg/min[24]. The TWR was calculated using $TWR = \frac{(W_i - W_f)}{T_m}$; where, W_i and W_f signify the initial and final weights of the tool in mg, respectively, and T_m is the total machining time in minutes. Tesa Rugosurf 10G surface roughness tester was used for the measurement of surface roughness on a cut-off length of 0.8 mm. The surface roughness values were taken at three locations on the

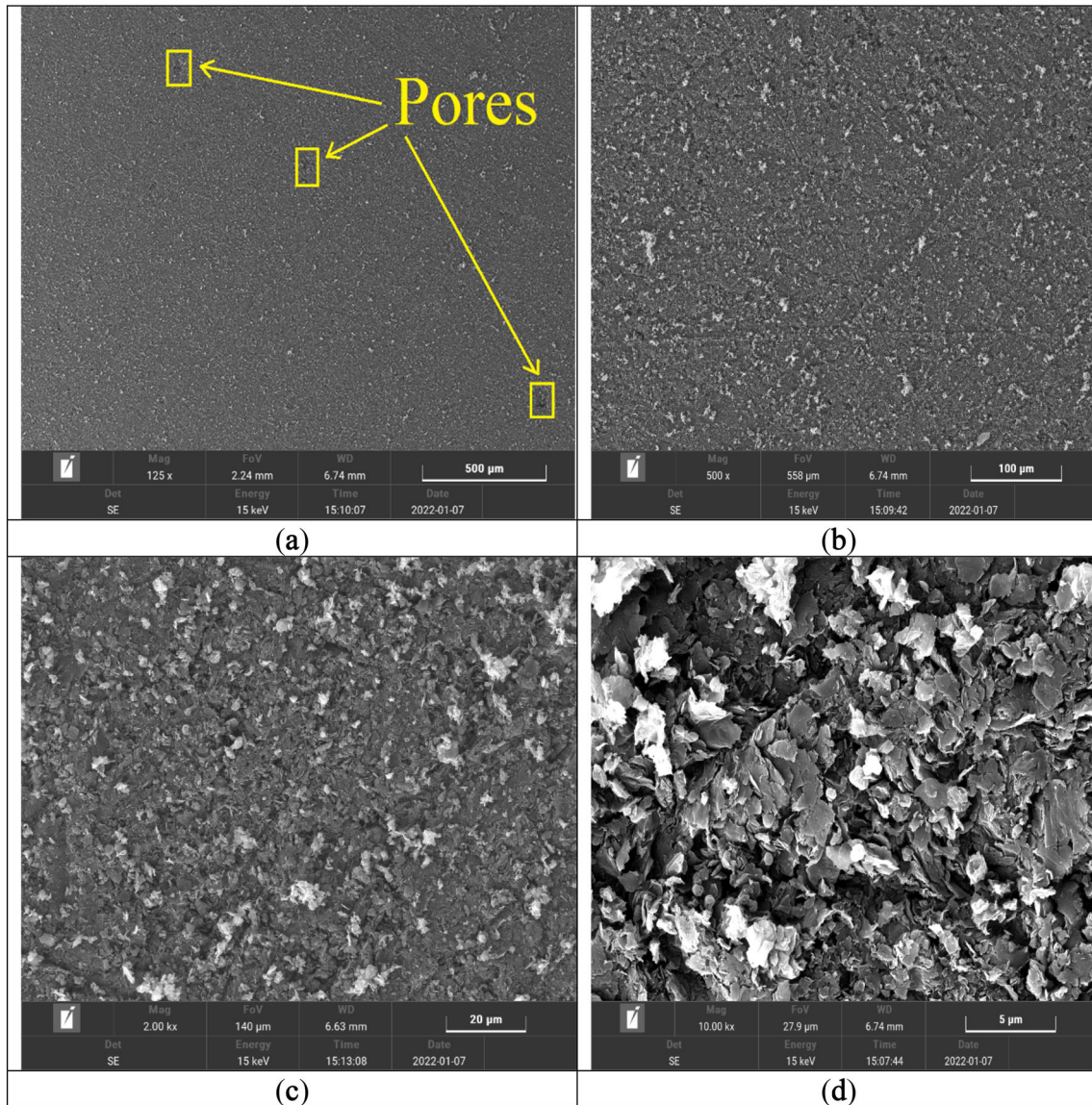


Figure 4. FESEM images of graphite tool at (a) 125x; (b) 500x; (c) 2kx; (d) 10kx.

machined surface in each experimental run and average of three values was taken to reduce variability.

2.5 Material hardening

The following process steps were used in hardening of EN31 steel.

- (i) Material was preheated at 750°C for 3 hours. This step was essential to avoid cracking.
- (ii) Material was then dipped in salt bath oil fired furnace (Neutral salt) at 1020°C for 90 minutes.
- (iii) Quenching in oil was done for 60 minutes.
- (iv) At last, tempering was done at 400°C for 4 hours.

The hardness obtained at final stage was 52 HRC on Brinell hardness tester.

2.6 Design of experiments and conduct of experimental runs

The experiments were planned using a 3^3 full factorial design. For studying 3 factors at 3 levels, 27 experiments were performed. The experimental runs were obtained through Minitab 17 software. The randomization of experimental run order suggested by software was done before starting the experiments. The randomization is an essential step to distribute randomly the variation due to noise. The Sparkonix 35A EDM machine was used for conducting the experiments. This study was performed on

Table 5. Properties of graphite and copper tool.

Property	Unit	Graphite	Copper
Bulk density	Mg/m ³	1.78	8.96 × 10 ⁹
Tensile strength	MPa	46	210 Ultimate 33.3 Yield
Hardness	HSD, Vickers	76 HSD	50 Vickers
Flexural strength	MPa	65	218
Electrical resistivity	μ Ω • m	15	0.01673
Coefficient of thermal expansion	10 ⁻⁶ /K	5.6	16.8
Young's modulus	GPa	12	116
Thermal conductivity	W/(m • K)	70	385
Compressive strength	MPa	135	206.84

Table 6. Experimental runs.

Run order	Process parameters			EN31 and Gr			EN31 and Cu		
	Pc (A)	Ton (μs)	Trpm (rpm)	MRR (mg/min)	TWR (mg/min)	SR (microns)	MRR (mg/min)	TWR (mg/min)	SR (microns)
1	18	100	1200	632.5	73.2	8.942	440.35	160.55	10.141
2	24	1000	1800	227.8	33.95	10.568	402.95	55.65	18.323
3	12	100	1500	333	107.4	8.237	118.5	61.25	7.499
4	12	400	1200	373.1	43.7	12.454	385.4	49.9	10.392
5	24	400	1200	502.4	17.4	13.263	890.7	158.45	17.613
6	24	400	1800	500	70.2	12.159	588.1	151.4	17.003
7	12	400	1800	390.8	117.4	10.468	180.4	39.4	12.256
8	18	100	1800	701.7	147.7	8.258	284.45	170.5	8.23
9	18	1000	1800	266.4	43.1	10.183	347.1	18.65	14.374
10	24	1000	1500	216.8	26.4	11.428	347.4	18.1	20.655
11	18	400	1500	547.9	73.3	11.59	410.7	102.45	12.508
12	24	100	1500	823.3	100.4	8.344	549.45	254.6	10.583
13	18	400	1200	544.4	46.9	11.842	630.75	68.65	12.917
14	12	1000	1200	245.9	29.4	11.178	337.6	37.9	10.64
15	24	100	1200	783.8	64.4	8.371	665.8	267.6	7.501
16	18	1000	1200	262.9	11.7	11.569	540.55	21.6	12.545
17	12	1000	1800	255.9	95.5	9.254	282.65	34.1	11.835
18	18	400	1800	545.3	98.5	11.23	496.65	94.1	14.58
19	18	100	1500	716.9	84.3	8.723	189.15	115.9	7.115
20	12	100	1800	308.5	151.3	7.859	130.7	56.2	5.944
21	24	1000	1200	204.7	8.8	11.835	685.2	69.7	18.46
22	24	100	1800	710.8	102.6	8.262	468.35	272.4	6.858
23	12	100	1200	326.6	57.7	8.368	162.8	76.5	9.583
24	12	1000	1500	190.2	55.7	9.815	205.05	32.8	8.047
25	24	400	1500	543.9	34.5	12.881	641.5	135.6	14.809
26	18	1000	1500	292.9	27.2	10.979	293.5	20.56	16.758
27	12	400	1500	302	73.1	11.487	260.25	49.15	10.786

EN31 steel. The workpiece material, EN31 steel, was hardened to 52 HRC. The study was conducted using a graphite (ISO 63 grade, 76 HSD) [25] and copper tool electrode of 20 mm diameter each where facing of the tool was done before conducting each experiment. FESEM micrographs illustrated in figure 4 were used to perform an examination into the detection of pores in graphite tool. It was done to check the surface quality of graphite as it has a direct impact on the surface roughness of the machined

parts in EDM. For this, a sample of 10 mm diameter was prepared. Following that, facing was done to acquire the same surface condition as it had prior to each experiment in order to represent the right surface condition. Figure 4 depicts micrographs captured at low and high magnification ranging from 125x to 10kx. It may be clearly elucidated from figure 4 that overall quality of graphite is adequate, with few micro-pores with mean size of 24.87 μm (Image J software) as evident in figure 4(a). Some graphite flakes are

Table 7. ANOVA table for MRR (EN31 and Gr) (after removing insignificant interaction and square terms).

Source	DF	Adj. SS	Adj. MS	F	P
Regression	5	961673	192335	89.45	0.000
Pc	1	107735	107735	50.11	0.000
Ton	1	29142	29142	13.55	0.001
Trpm	1	53	53	0.02	0.877
Pc × Pc	1	58826	58826	27.36	0.000
Pc × Ton	1	147325	147325	68.52	0.000
Error	21	45152	2150		
Total	26				

DF: degree of freedom; Adj. SS: adjusted sum of squares; Adj. MS: adjusted mean square; F: Fisher's value.

Table 8. ANOVA table for TWR (EN31 and Gr) (after removing insignificant interactions and square terms).

Source	DF	Adj. SS	Adj. MS	F	P
Regression	6	37503.8	6250.6	53.59	0.000
Pc	1	531.4	531.4	4.56	0.045
Ton	1	359.2	359.2	3.08	0.095
Trpm	1	4701.5	4701.5	40.31	0.000
Ton × Ton	1	1174.9	1174.9	10.07	0.005
Pc × Trpm	1	1145.6	1145.6	9.82	0.005
Ton × Trpm	1	603.7	603.7	5.18	0.034
Error	20	2332.6	116.6		
Total	26				

DF: degree of freedom; Adj. SS: adjusted sum of squares; Adj. MS: adjusted mean square; F: Fisher's value.

Table 9. ANOVA table for SR (EN31 and Gr) (after removing insignificant interactions and square terms).

Source	DF	Adj. SS	Adj. MS	F	P
Regression	5	68.5389	13.7078	87.28	0.000
Pc	1	3.5476	3.5476	22.59	0.000
Ton	1	28.9963	28.9963	184.63	0.000
Trpm	1	0.4201	0.4201	2.68	0.117
Ton × Ton	1	44.1502	44.1502	281.11	0.000
Ton × Trpm	1	0.7750	0.7750	4.93	0.037
Error	21	3.2982	0.1571		
Total	26	71.8370			

DF: degree of freedom; Adj. SS: adjusted sum of squares; Adj. MS: adjusted mean square; F: Fisher's value.

seen as bright spots in figure 4(b), which is more obvious in figures 4(c and d). Table 5 further shows that the properties of the graphite tool utilised in this study are found in moderate range with adequate bulk density, hardness, and compressive strength. The machining time was kept constant for a period of 2 minutes for each experiment. The pulse off time was kept constant at 30 μ s. The experiments were repeated three times on same levels of the parameters. The experimental results along with run order for MRR, TWR and SR are presented in table 6 for both tool material combination.

3. Statistical modeling of process responses

ANOVA was done to quantify the variance due to process parameters and uncontrollable factors along with the percentage share of different parameters on machining responses. A confidence interval of 95% was used. The statistical models were generated for MRR, TWR and SR in machining of EN31 steel with graphite and copper electrode through regression equations with the help of Minitab 17 software. The uncontrollable factors during

Table 10. ANOVA table for MRR (EN31 and Cu) (after removing insignificant interactions and square terms).

Source	DF	Adj. SS	Adj. MS	F	P
Regression	6	933087	155514	44.31	0.000
Pc	1	380009	380009	108.28	0.000
Ton	1	169531	169531	48.31	0.000
Trpm	1	77209	77209	22.00	0.000
Ton × Ton	1	126493	126493	36.04	0.000
Trpm × Trpm	1	66115	66115	18.84	0.000
Pc × Ton	1	43988	43988	12.53	0.002
Error	20	70190	3509		
Total	26				

DF: degree of freedom; Adj. SS: adjusted sum of squares; Adj. MS: adjusted mean square; F: Fisher’s value.

Table 11. ANOVA table for TWR (EN31 and Cu) (after removing insignificant interactions and square terms).

Source	DF	Adj. SS	Adj. MS	F	P
Regression	5	145427	29085.5	84.50	0.000
Pc	1	67886	67886.3	197.23	0.000
Ton	1	28	27.6	0.08	0.780
Trpm	1	19	18.9	0.05	0.817
Ton × Ton	1	3178	3177.7	9.23	0.006
Pc × Ton	1	25127	25127.1	73.00	0.000
Error	21	7228	344.2		
Total	26				

DF: degree of freedom; Adj. SS: adjusted sum of squares; Adj. MS: adjusted mean square; F: Fisher’s value.

experimentation led to the difference between the model output and experimented data.

3.1 EN31 and Gr

ANOVA results for MRR, TWR and SR in machining of EN31 steel with graphite electrode are shown in tables 7, 8 and 9, respectively. These tables consist of data after removing insignificant interactions and square terms. Equations (1), (2) and (3) are regression equations for MRR, TWR and SR, respectively. The R²_{adjusted} for MRR, TWR and SR are 94.45%, 92.39% and 94.32%, respectively which showed good fit for model.

$$\begin{aligned}
 \text{MRR} = & -864.0 + (135.7 \times P_c) + (0.3343 \times T_{on}) \\
 & + (0.0057 \times T_{rpm}) - (2.750 \times P_c^2) \\
 & - (0.04030 \times P_c \times T_{on}) \tag{1}
 \end{aligned}$$

Table 12. ANOVA table for SR (EN31 and Cu) (after removing insignificant interactions and square terms).

Source	DF	Adj. SS	Adj. MS	F	P
Regression	5	379.103	75.8206	30.43	0.000
Pc	1	0.541	0.5407	0.22	0.646
Ton	1	19.084	19.0838	7.66	0.012
Trpm	1	0.008	0.0084	0.00	0.954
Ton × Ton	1	64.353	64.3529	25.83	0.000
Pc × Ton	1	48.827	48.8268	19.6	0.000
Error	21	52.317	2.4913		
Total	26				

DF: degree of freedom; Adj. SS: adjusted sum of squares; Adj. MS: adjusted mean square; F: Fisher’s value.

$$\begin{aligned}
 \text{TWR} = & -167.1 + (5.62 \times P_c) - (0.0785 \times T_{on}) \\
 & + (0.2174 \times T_{rpm}) + (0.000079 \times T_{on}^2) \\
 & - (0.00543 \times P_c \times T_{rpm}) \\
 & - (0.000052 \times T_{on} \times T_{rpm}) \tag{2}
 \end{aligned}$$

$$\begin{aligned}
 \text{SR} = & 6.518 + (0.0740 \times P_c) + (0.02230 \times T_{on}) \\
 & - (0.000850 \times T_{rpm}) - (0.000015 \times T_{on}^2) \\
 & - (0.000002 \times T_{on} \times T_{rpm}) \tag{3}
 \end{aligned}$$

3.2 EN31 and Cu

ANOVA results for MRR, TWR and SR in machining of EN31 steel with copper electrode are shown in tables 10, 11 and 12, respectively. The regression equations for MRR, TWR and SR are shown in equations (4), (5) and (6), respectively. The R²_{adjusted} for MRR, TWR and SR are 90.91%, 94.14% and 84.99%, respectively which showed good fit for model.

$$\begin{aligned}
 \text{MRR} = & 2506.0 + (40.42 \times P_c) + (1.353 \times T_{on}) \\
 & - (3.788 \times T_{rpm}) - (0.000821 \times T_{on}^2) \\
 & + (0.001166 \times T_{rpm}^2) - (0.02202 \times P_c \times T_{on}) \tag{4}
 \end{aligned}$$

$$\begin{aligned}
 \text{TWR} = & -115.9 + (17.08 \times P_c) + (0.0173 \times T_{on}) \\
 & - (0.0034 \times T_{rpm}) + (0.000130 \times T_{on}^2) \\
 & - (0.01664 \times P_c \times T_{on}) \tag{5}
 \end{aligned}$$

$$\begin{aligned}
 \text{SR} = & 4.83 + (0.048 \times P_c) + (0.01436 \times T_{on}) \\
 & - (0.00007 \times T_{rpm}) - (0.000019 \times T_{on}^2) \\
 & + (0.000734 \times P_c \times T_{on}) \tag{6}
 \end{aligned}$$

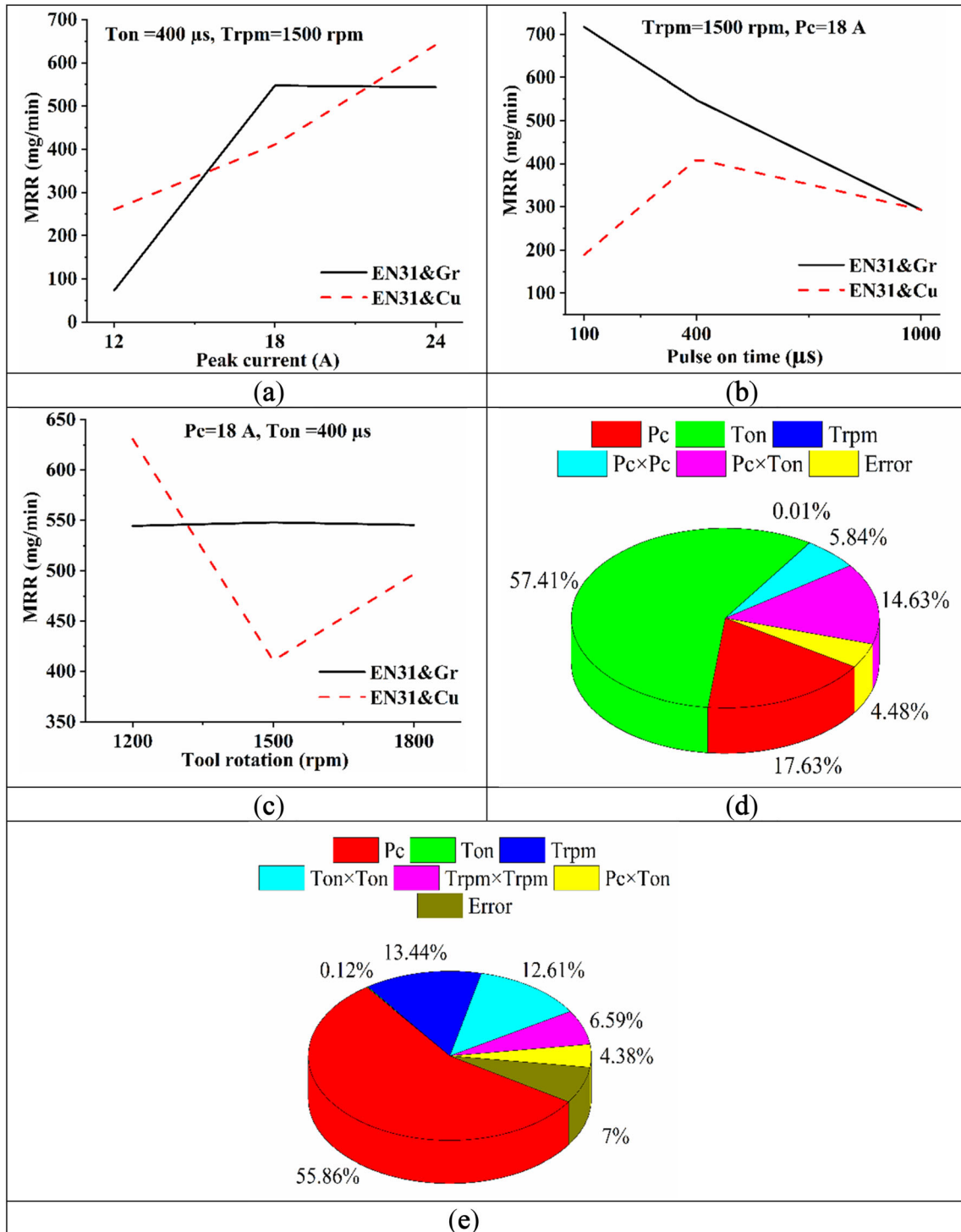


Figure 5. Actual plots showing effect of (a) peak current; (b) pulse on time; (c) tool rotation on MRR in EN31 and Gr and EN31 and Cu; (d) parameters percentage share on MRR in EN31 and Gr; (e) parameters percentage share on MRR in EN31 and Cu.

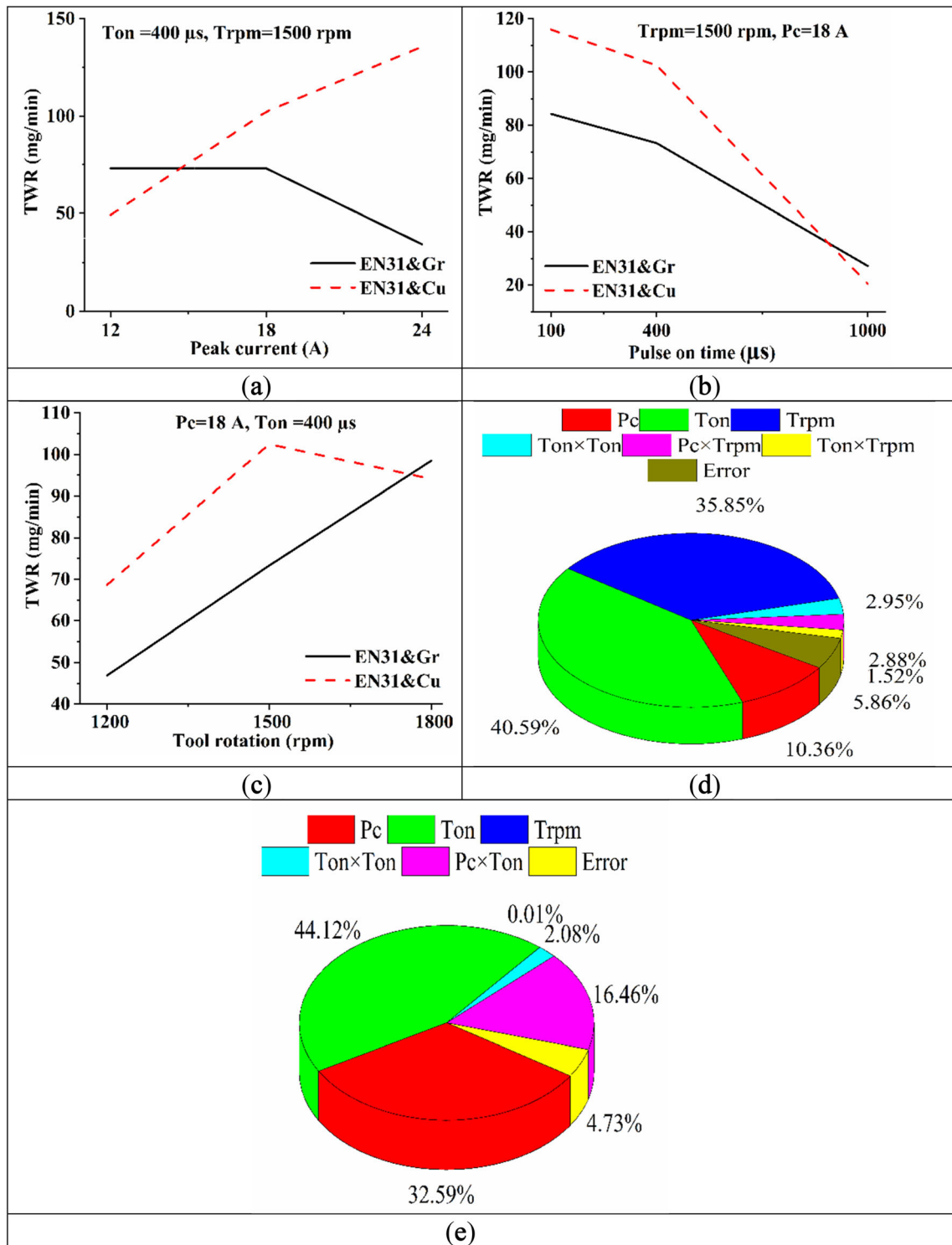


Figure 6. Actual plots showing effect of (a) peak current; (b) pulse on time; (c) tool rotation on TWR in EN31 and Gr and EN31 and Cu; (d) parameters percentage share on TWR in EN31 and Gr; (e) parameters percentage share on TWR in EN31 and Cu.

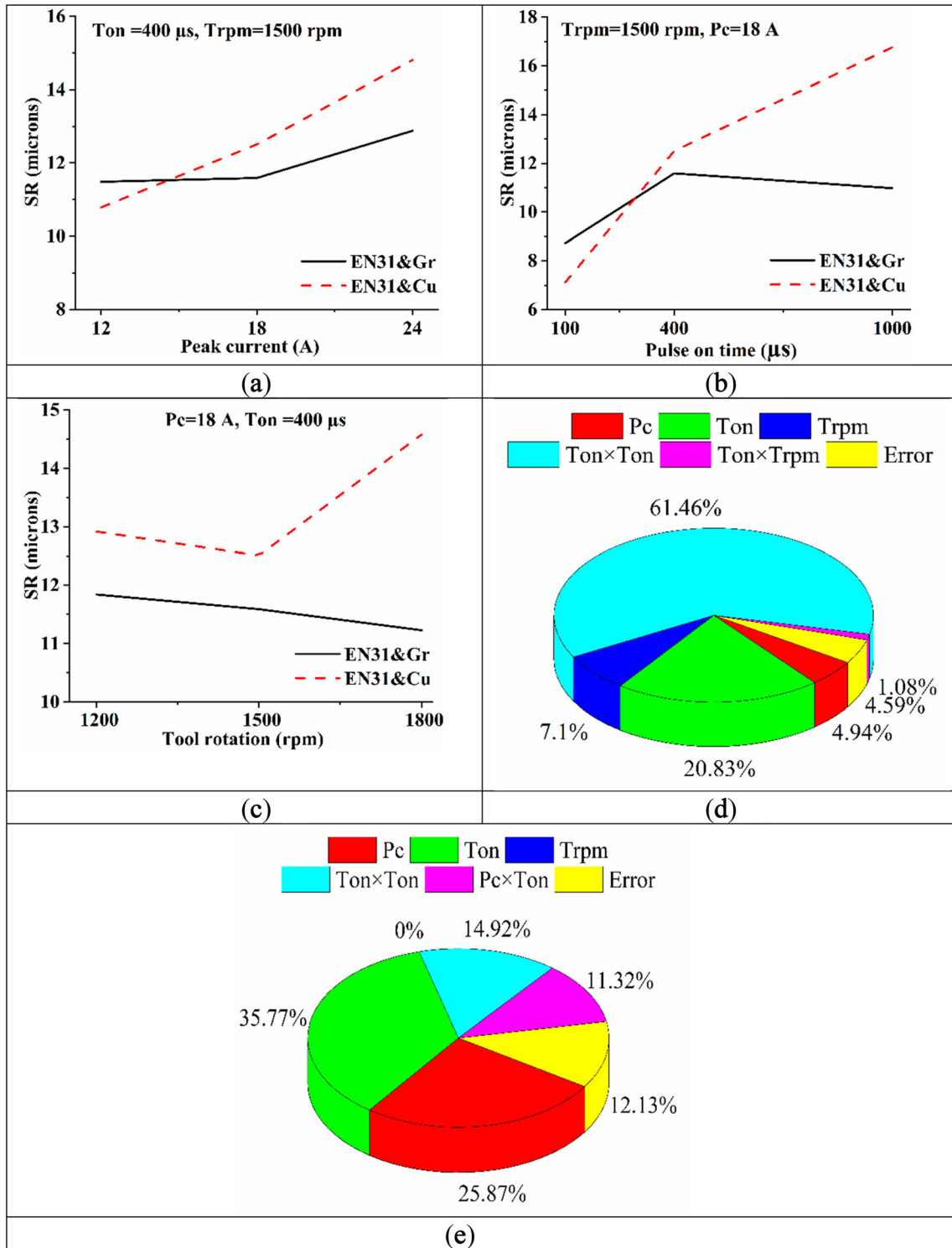


Figure 7. Actual plots showing effect of (a) peak current; (b) pulse on time; (c) tool rotation on SR in EN31 and Gr and EN31 and Cu; (d) parameters percentage share on SR in EN31 and Gr; (e) parameters percentage share on SR in EN31 and Cu.

Table 13. Response table for MRR, TWR and SR.

O/p	W/p and tool	Input parameters								
		Pc (A)			Ton (μ s)			Trpm (rpm)		
		12	18	24	100	400	1000	1200	1500	1800
MRR	EN31&Gr	302.9	501.2	501.5	593	472.2	240.4	430.7	440.8	434.1
	EN31&Cu	229.3	403.7	582.2	334.4	498.3	382.4	526.6	335.1	353.5
TWR	EN31&Gr	81.24	67.32	50.96	98.78	63.89	36.86	39.24	64.70	95.58
	EN31&Cu	48.58	85.88	153.72	159.5	94.34	34.34	101.21	87.82	99.16
SR	EN31&Gr	9.9	10.36	10.79	8.37	11.93	10.75	10.86	10.38	9.8
	EN31&Cu	9.66	12.13	14.64	8.16	13.65	14.62	12.19	12.08	12.15

O/p: output responses; W/p: workpiece material.

4. Results and discussion

The following segment explains the result of different process parameters as well as their interactions on the performance measures. Figures 5, 6 and 7 show the actual plot and percentage share by each parameter on material removal rate, tool wear rate and surface roughness in EN31 and Gr and EN31 and Cu, respectively. These plots are created by taking one variable at a time and setting the other two at their mid values (refer table 13 for mean response values).

4.1 Effect of process parameters on MRR

Figures 5(a, b, c) and 8(a, b, c) show the effect of peak current, pulse on time and tool rotation on MRR in machining of EN31 steel with graphite and copper electrode, respectively. Peak current is the maximum current that flows during each pulse. The material removal rate increased with increase in current for both electrodes. At high current, energy density of spark increases leading to more melting and vaporization of the material. As a result, material removal rate increases. The material removal rate with graphite was found to be more during current interval from 12 to 18 A but copper takes over from 18 to 24 A in which the graphite electrode showed a flat response. In the first half, the graphite electrode performs better than the copper electrode because of its low thermal conductivity (70 W/m·K)[25] and high melting temperature. Due to this, a stable arc is formed as the sideways dissipation of heat is less. With copper electrode, thermal conductivity being high (385 W/m·K)[26], heat dissipation is more than that of graphite. Hence, for same current, less heat is transferred to work surface leading to less MRR. In the second half i.e. during high current interval, the electrical conductivity of copper (5.96×10^7 S/m at 20°C) [27] which is very high than that of graphite (2 to 3×10^5 S/m at 20°C) [27]

outperforms the thermal conductivity effects. Due to high electrical conductivity, copper electrode effectively conducts the electric charge leading to high MRR. On the contrary, graphite fails to apprehend MRR at high current because at high current, temperature becomes high which reduces the electrical conductivity owing to more vibration and movement between molecules which obstructs in the route of current flow. A comparative bar graph showing the effect of peak current on MRR for both electrodes is shown in figure 8(a). Figure 5(e) shows that peak current was the most influencing factor in MRR with a percentage of 55.86% with copper electrode.

Pulse on time is the time for which current flows into the circuit. In the first interval, MRR decreased with the graphite electrode i.e. from 100 to 400 μ s and increased with the copper electrode. Then, in the second interval i.e. from 400 to 1000 μ s, the value decreased in both cases but the rate of decrease was more rapid with the graphite electrode. At low pulse on time i.e. at 100 μ s, arc is highly stable (cylindrical arc) with both electrodes but low MRR was recorded for copper electrode owing to its high thermal conductivity, less heat goes into the work leading to less MRR whereas graphite electrode recorded a high MRR because of its low thermal conductivity leading to more heat transfer to work and hence higher MRR. At 400 μ s, cylindrical arc changes to a convex arc because of considerably higher pulse on time than off time which is the reason for its expansion in the longitudinal direction (longitudinal direction here refers to the direction parallel to the top surface of workpiece) due to more heat [28]. Hence, heat loss increases in longitudinal direction compared to cylindrical arc. Now, at this value, MRR reduced for graphite electrode because of this additional heat loss due to convex arc. On the other hand, MRR increased for copper electrode because of its high electrical conductivity which encompasses the loss done by convex arc in longitudinal direction. At 1000 μ s, pulse off time (30 μ s) became very small compared to on time. At this stage, short circuiting

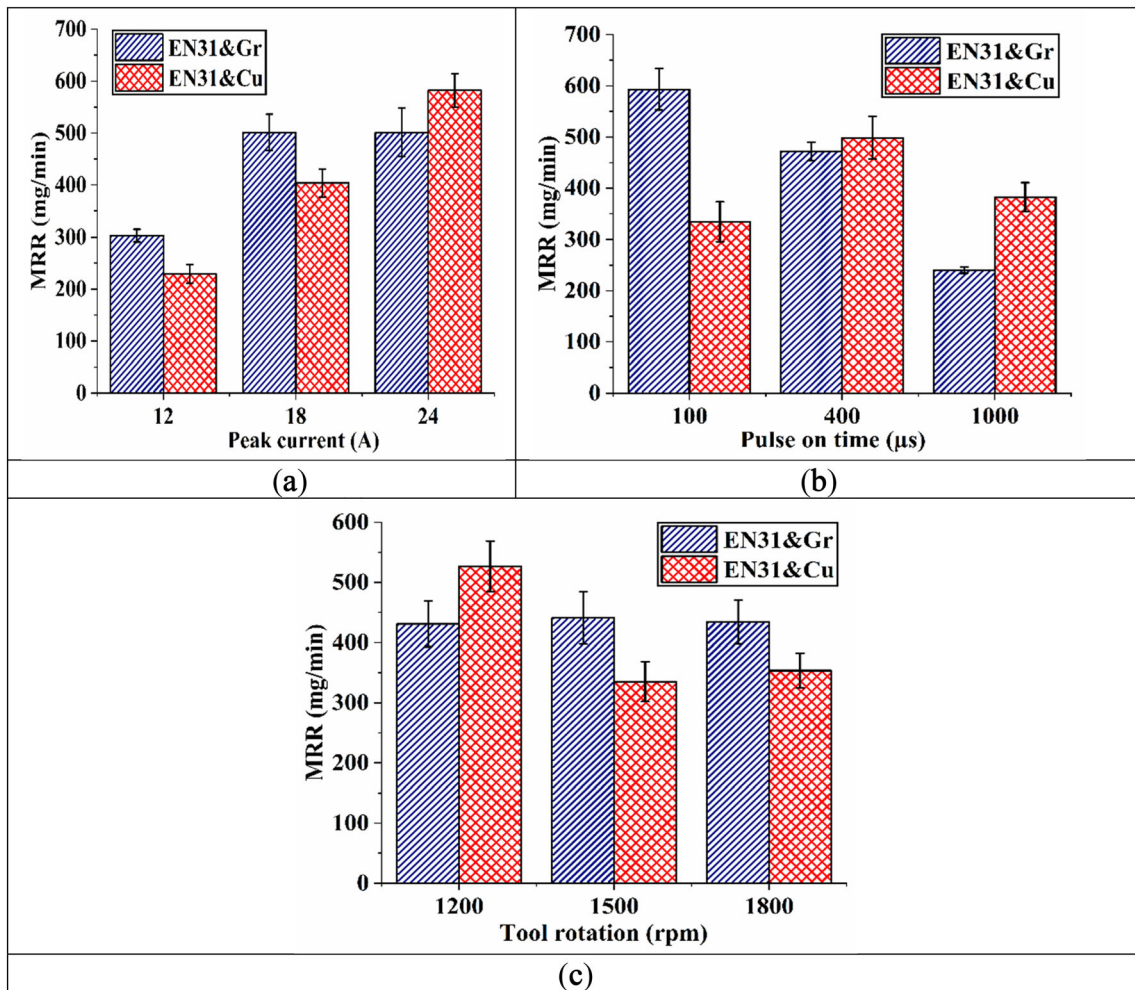


Figure 8. Bar graph showing effect of (a) peak current; (b) pulse on time; (c) tool rotation on MRR of EN31 steel machined with graphite and copper electrode.

was noticed with both electrodes. This might be because the dielectric fluid does not have enough time to deionize. Figure 5(d) shows that pulse on time is the most influencing factor in MRR with a percentage of 57.41% in graphite electrodes.

Tool rotation refers to different rotational speeds of tool. The material removal rate remained almost same at different rotational speeds of graphite electrode while in case of copper, it decreased in the first interval i.e. from 1200 to 1500 rpm and then increased in second interval i.e. from 1500 to 1800 rpm. The graphite electrode being less thermally conductive was not sufficiently augmented by tool rotation and hence recorded no appreciable improvements in MRR. The decrease of MRR with copper electrode is again attributed to its high thermal conductivity (5.5 times greater than graphite electrode). The high thermal conductivity of copper was augmented by tool rotation effects leading to more sideways heat dissipation. This led to less heat transfer rate to work and hence recorded less MRR, although small increase was noticed beyond 1500 rpm.

4.2 Effect of process parameters on TWR

Figures 6(a, b, c) and 9(a, b, c) show the effect of peak current, pulse on time and tool rotation on TWR in machining of EN31 steel with graphite and copper electrode, respectively. The TWR decreased with increase in peak current with graphite electrode while it increased with copper electrode. Figure 6(d) showed that the pulse on time contributed maximum (40.59%) for TWR with graphite. On careful observation of table 6, it is inferred that combination of high current (24 A) and pulse on time (1000 μs) resulted in very low TWR particularly for graphite. As explained earlier, graphite underwent more erratic cycling and short circuiting which led to material deposition on its surface and hence, reduced TWR.

The TWR of both electrode was found to decrease with pulse on time. This is due to the reduction in tool tip temperature due to the expansion of plasma at higher pulse on time. Moreover, it was observed during experimentation that carbon deposits increased on high pulse on time, particularly on 1000 μs. The carbon decomposition from

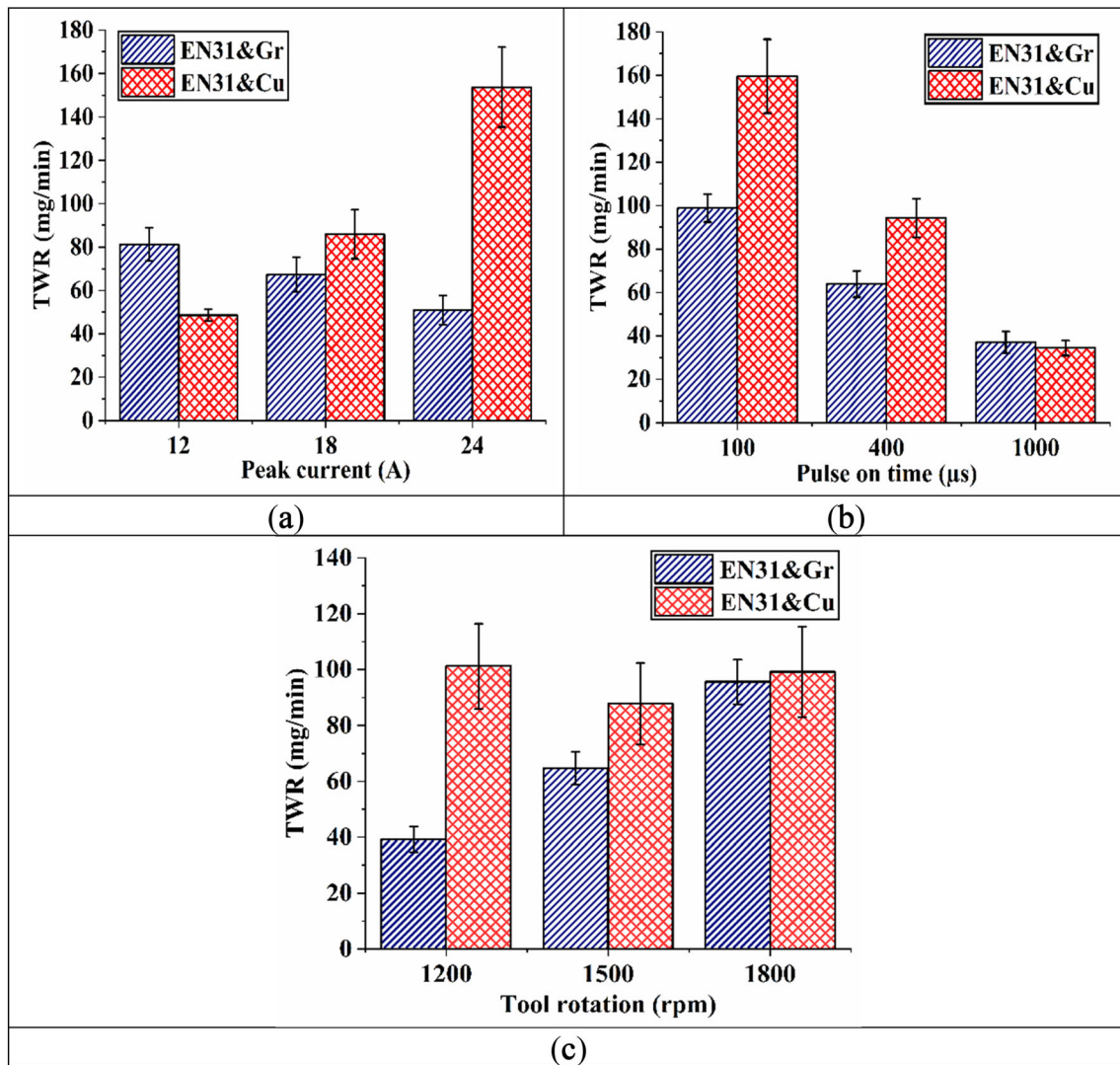


Figure 9. Bar graph showing effect of (a) peak current; (b) pulse on time; (c) tool rotation on TWR of EN31 steel machined with graphite and copper electrode.

dielectric fluid on tool surface provided the protection against wear under pyrolysis process [29]. Hence, reduction in tool tip temperature and added carbon layer led to less TWR at high pulse on time.

The increase in tool rotation resulted in increase of TWR with graphite electrode while the effect with copper electrode remained same as that of graphite i.e. increased in first half but, later on, recorded a small decline.

Figures 6(d, e) show the percentage share by each parameter on TWR in EN31 and Gr and EN31 and Cu, respectively. The pulse on time and tool rotation were found to be most influencing factors with 40.59% and 35.85%, respectively for graphite electrode. In case of copper electrodes, pulse on time and peak current were found to be most influencing factors with 44.12% and 32.59%, respectively.

4.3 Effect of process parameters on SR

Figures 7(a, b, c) and 10(a, b, c) show the effect of process parameters on surface roughness of EN31 steel. The surface roughness increased with increase in current for both the electrode, however, the increase with copper electrode was more compared to graphite electrode. At high value of current, energy density of spark is high and hence crater formed in the workpiece is larger. As a result, the surface roughness value increases.

The pulse on time is also critical parameter affecting surface roughness. The surface roughness increased with increase in pulse duration; however, it decreased from 400 to 1000 μ s in case of graphite electrode. The cumulative effects of peak current and pulse on time were seen on surface roughness by observing a clear dark circle near centre indicating carbon deposit with copper electrode. This

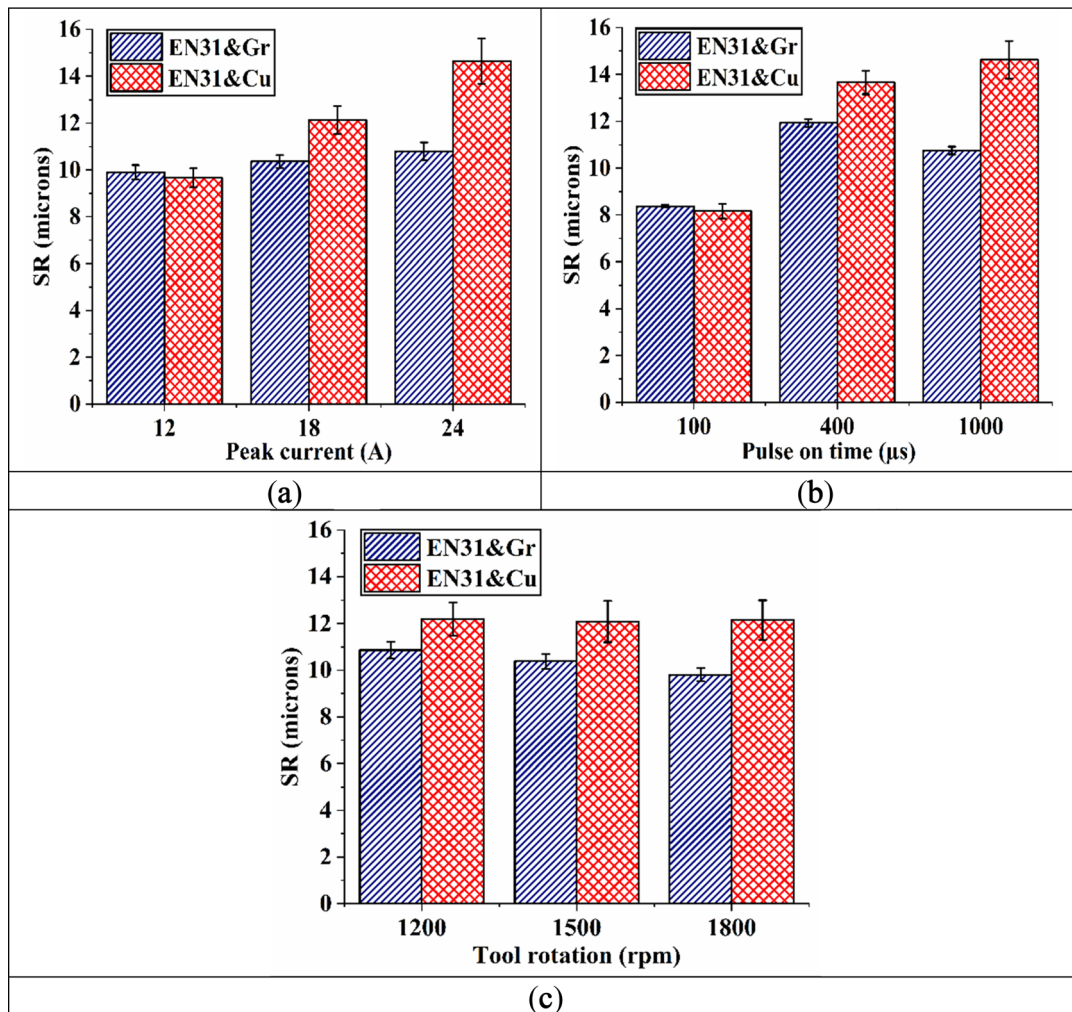


Figure 10. Bar graph showing effect of (a) peak current; (b) pulse on time; (c) tool rotation on SR of EN31 steel machined with graphite and copper electrode.

deposited carbon resulted in high surface roughness. It was also observed during experimentation that the extent of carbon deposition increased from mid to high value of peak current and pulse on time.

Surface roughness increased with increase in tool rotation with a minor dip at 1500 rpm for copper electrode and reduced for graphite electrode. Tool rotation has contributed in better flushing with graphite electrode resulting in better surface finish.

The pulse on time was the most influencing factor for graphite and copper electrode with percentage of 20.83% and 35.77%, respectively (refer figures 7(d, e)).

4.4 Interaction effect in EN31 and Gr

The interaction effects of peak current and pulse on time on MRR, peak current and tool rotation on TWR, pulse on time and tool rotation on TWR, pulse on time and tool

rotation on SR were found to be significant in EN31 steel machined with graphite electrode.

4.4a Interaction effect on MRR: Figure 11 shows the surface and interaction plot of peak current and pulse on time on MRR. The low level of pulse on time and high level of current resulted in maximum MRR. The reason is attributed to the fact that the combination of these two levels makes the arc highly concentrated over the workpiece leading to maximum heat input into the workpiece and, hence, high MRR.

4.4b Interaction effect on TWR: Figure 12 shows the surface and interaction plot of peak current and tool rotation on TWR. The peak current affected TWR in inverse proportion for all tool rotation value. The effect of increase in peak current resulted in the reduction of TWR. With an increase in tool rotation, slope of the line was also increased. The lowest TWR occurred at high value of peak current and low value of tool rotation as at high value of

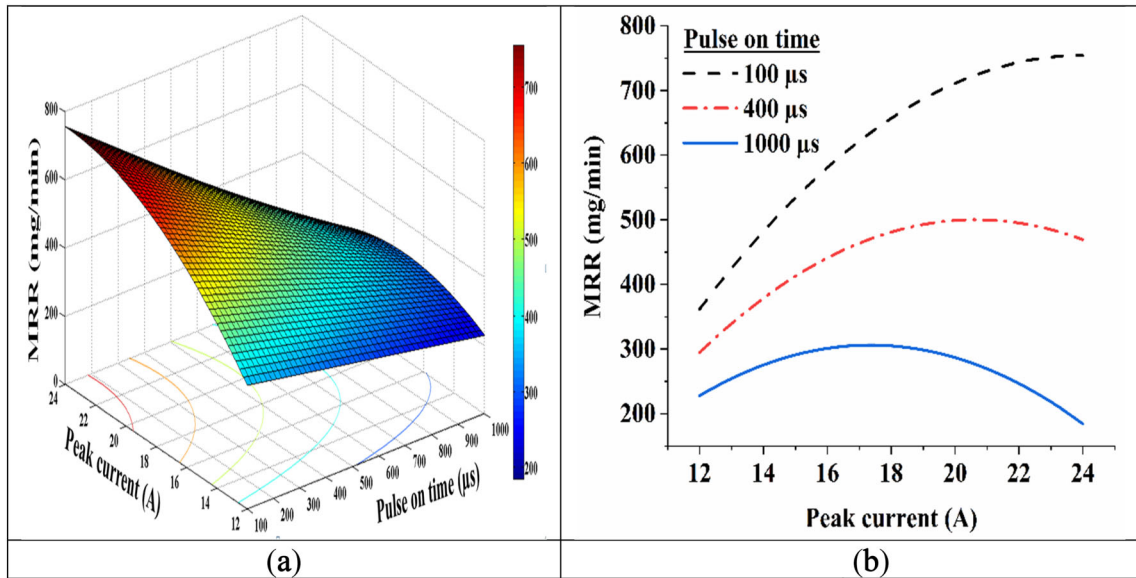


Figure 11. Effect of peak current and pulse on time on MRR in EN31 and Gr: (a) response surface plot; (b) interaction plot.

peak current, energy density of spark is high but at the same time tool rotation changes the concentricity of spark column to the formation of bulge at the centre making the distribution of temperature uneven at ends and at centre. Due to this phenomenon, tool tip temperature decreases leading to less wear on surface and, hence, less TWR.

Figure 13 shows the surface and interaction plot of pulse on time and tool rotation on TWR. The pulse on time also showed the inversely proportional effects on TWR for given tool rotation values. The lowest TWR was found on

high value of pulse on time and low value of tool rotation. The reason for low TWR was a reduction in tool tip temperature due to expansion of plasma channel at high levels of pulse on time.

4.4c Interaction effect on SR Figure 14 shows the surface and interaction plot of pulse on time and tool rotation on SR. The surface roughness increased in first half then decreased in second half with increase in pulse of time for all levels of tool rotation. The lowest surface roughness

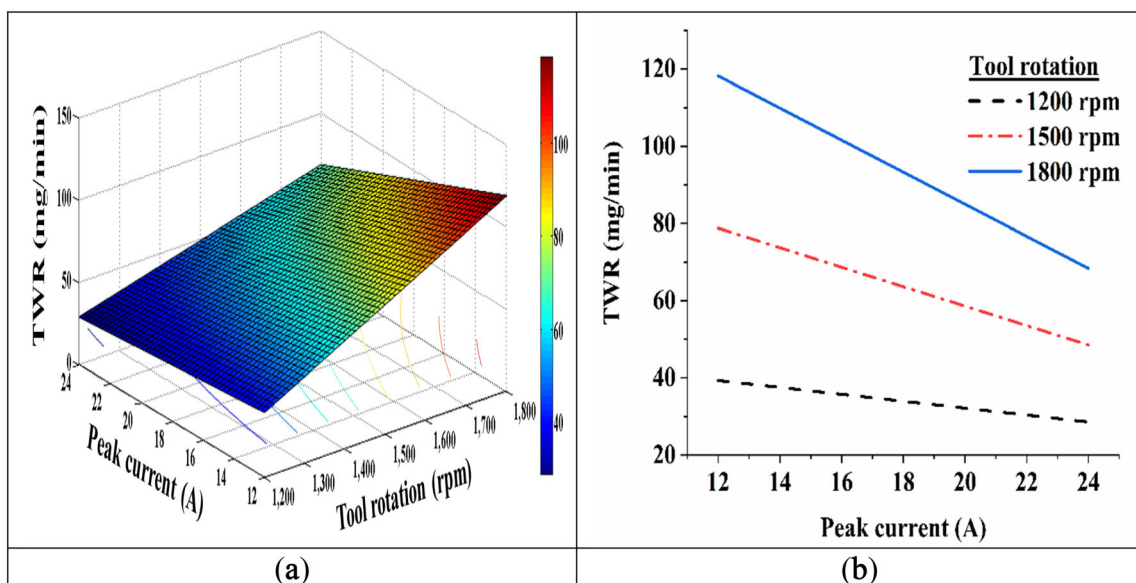


Figure 12. Effect of peak current and tool rotation on TWR in EN31 and Gr: (a) response surface plot; (b) interaction plot.

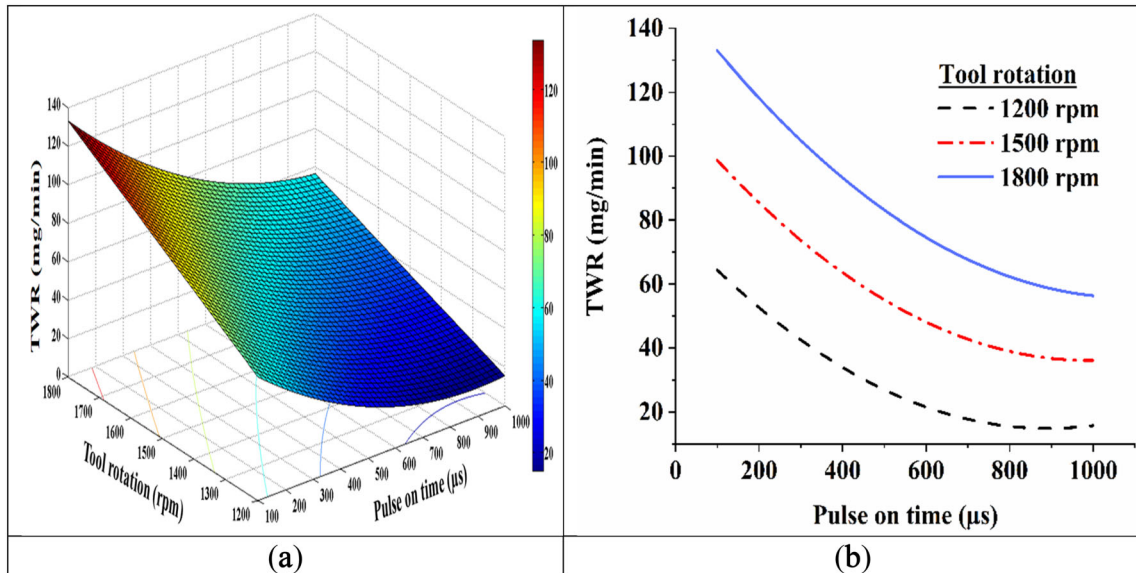


Figure 13. Effect of pulse on time and tool rotation on TWR in EN31 and Gr: (a) response surface plot; (b) interaction plot.

recorded at low level of pulse on time and high level of tool rotation. The reason is attributed to low intensity of spark at low level of pulse on time and effective debris removal with higher rotation. The higher tool rotational speed helped in cleaning the inter-electrode gap (refer figure 14 (a)). Due to this effective cleaning, re-solidified spots were not formed which otherwise would have been formed and would have increased roughness.

4.5 Interaction effect in EN31 and Cu

The interaction effects of peak current and pulse on time on MRR, peak current and pulse on time on TWR, peak current and pulse on time on SR were found significant in machining of EN31 steel with copper electrode.

4.5a Interaction effect on MRR: Figure 15 shows the surface and interaction plot of peak current and pulse on

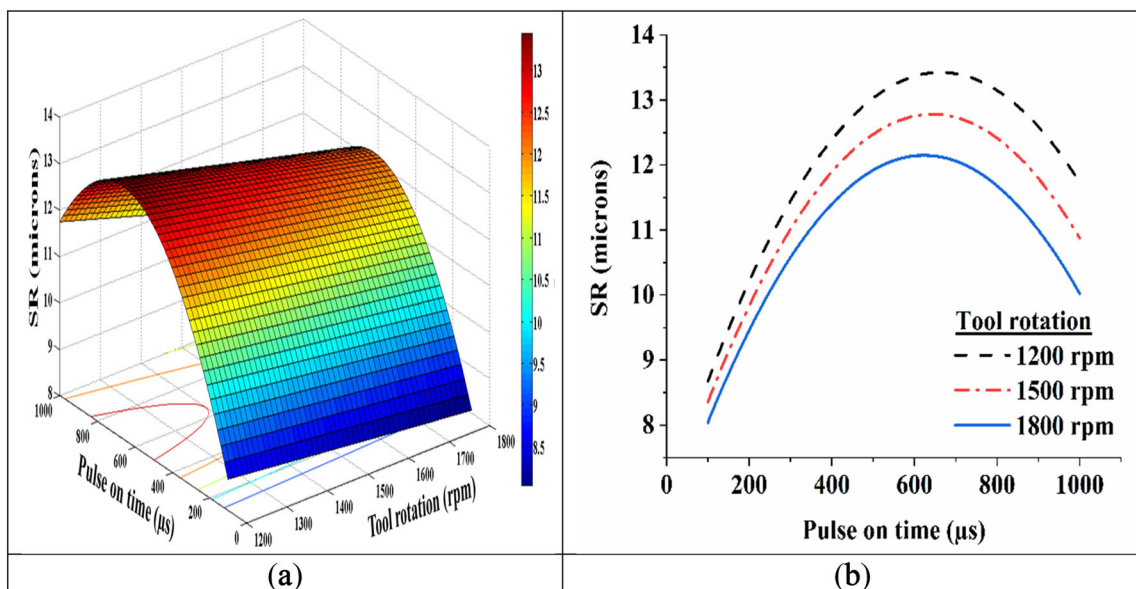


Figure 14. Effect of pulse on time and tool rotation on SR in EN31 and Gr: (a) response surface plot; (b) interaction plot.

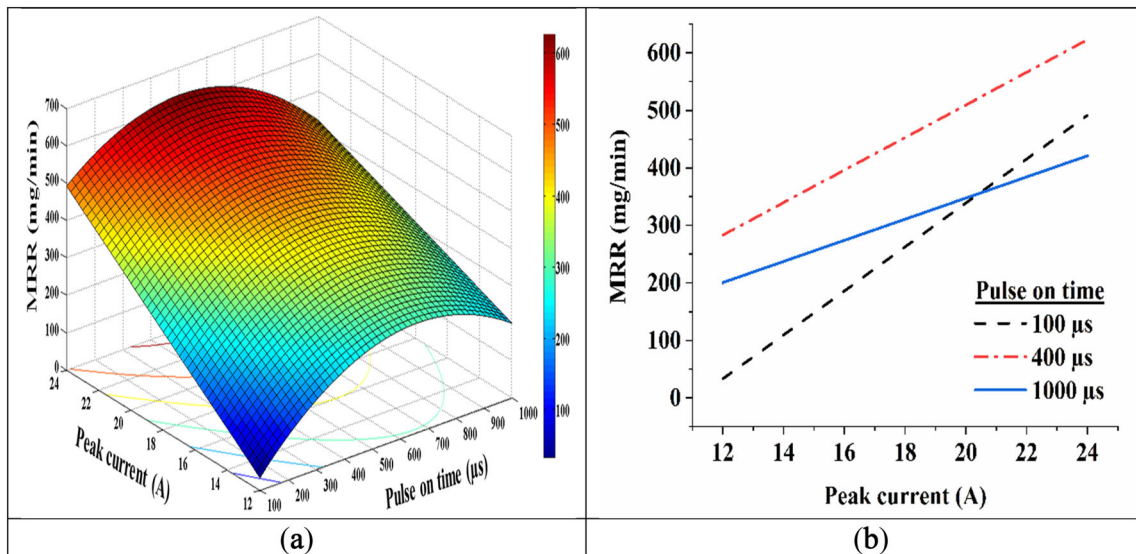


Figure 15. Effect of peak current and pulse on time on MRR in EN31 and Cu: (a) response surface plot; (b) interaction plot.

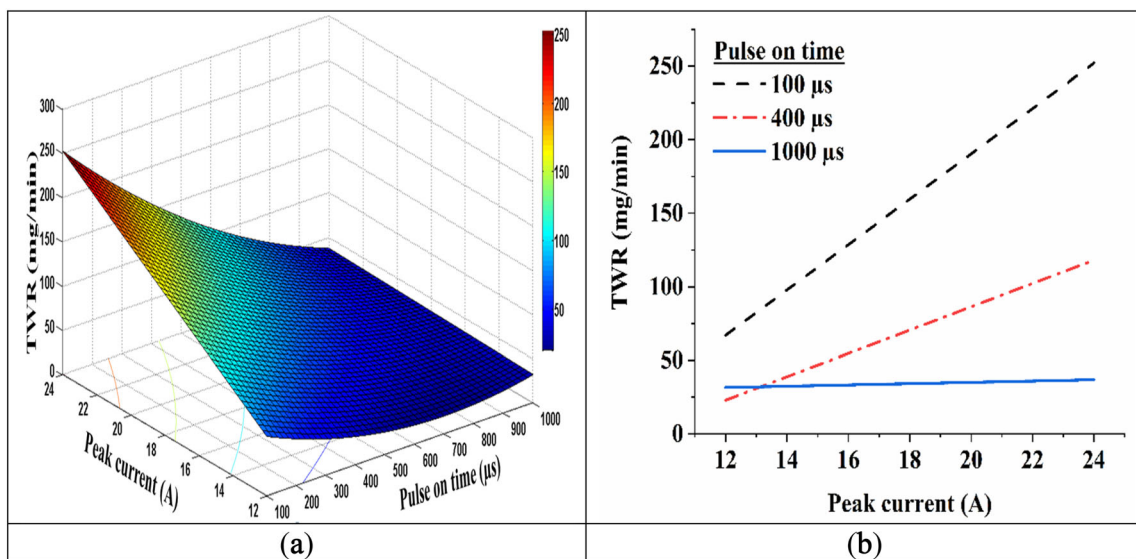


Figure 16. Effect of peak current and pulse on time on TWR in EN31 and Cu: (a) response surface plot; (b) interaction plot.

time on MRR. The peak current effected MRR in direct proportion as MRR increased with increase in peak current for all levels of pulse on time. The largest slope was recorded on 100 μs, then reduced on 400 μs and lowest on 1000 μs. The maximum MRR was recorded on high level of current and intermediate level of pulse on time. The reason for decrease in slope with an increase in pulse on time is the expansion of plasma in longitudinal direction which decreases the energy density of spark.

4.5b Interaction effect on TWR: The TWR was also found to be affected by interaction of peak current and pulse on

time, shown in figure 16. The slope of the line decreased from first to the third level of pulse on time which almost approximated to zero slope at third level. The lowest TWR was recorded at high level of current and high level of pulse on time. The reason for lowest TWR at this combination is attributed to decrease in tool tip temperature as a result of plasma expansion leading to less temperature and hence less electrode wear.

4.5c Interaction effect on SR: The peak current and pulse on time interaction effect remained consistently prominent for surface roughness as it was for MRR and TWR, shown

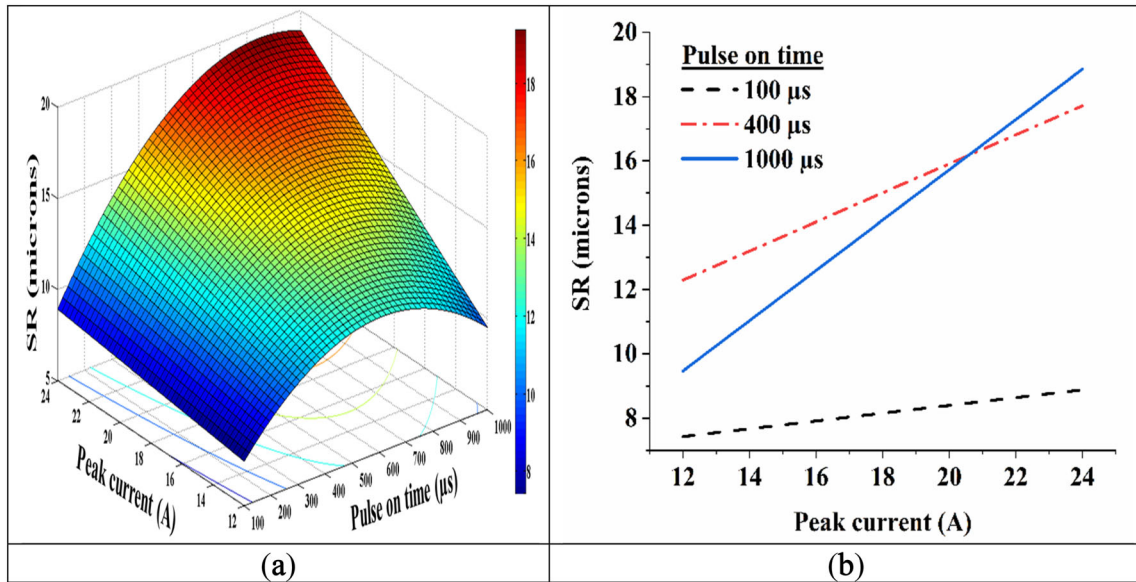


Figure 17. Effect of peak current and pulse on time on SR in EN31 and Cu: (a) response surface plot; (b) interaction plot.

in figure 17. The surface roughness was found in direct proportion to peak current for all pulse on time levels. The surface roughness was found lowest at low level of peak current and low level of pulse on time. The reason for lowest surface roughness at this combination is low energy density of spark which results in shallow craters.

5. Analysis of voltage and current waveforms

The voltage and current waveforms were recorded with the help of Keysight Digital Storage Oscilloscope DSO-X 2022A. The voltage and current probes were used to record

the voltage and current waveforms. The recorded waveforms are presented in figure 18. The spark cycle observed in the case of graphite electrode, figure 18(a), was found to be uniform without any disturbance while in case of copper, figure 18(b), spark cycle differences were quite obvious. In figure 18(b), the ignition delay time in peak 2 among all was largest showing delayed sparking. The delay in sparking will affect the machining rate. The same may be verified from the results in table 6 as well as figures 5 (a, b, c). At run order 11 of table 6, MRR recorded with graphite tool (547.9 mg/min) was higher than that of copper electrode (410.7 mg/min).

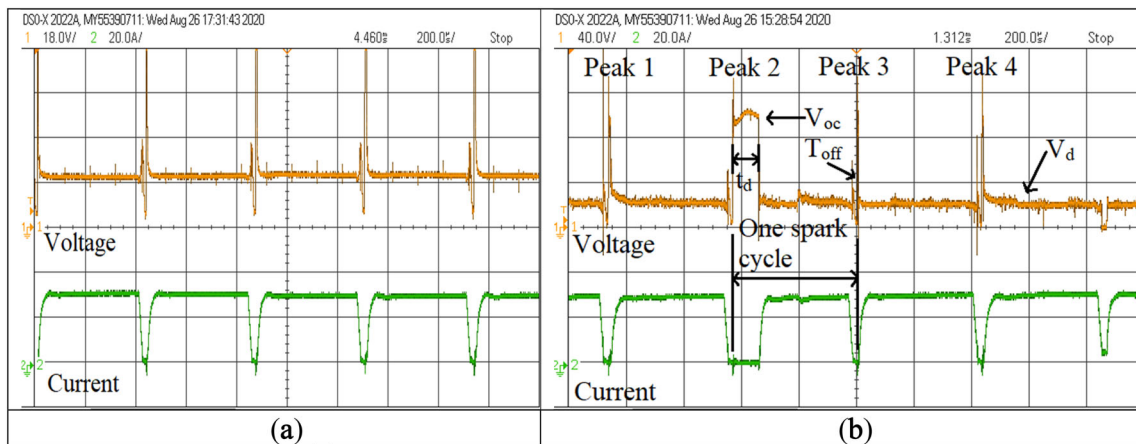


Figure 18. Voltage and current waveforms during (a) EN31 and Gr; (b) EN31 and Cu. (V_{oc} -open circuit voltage, V_d - discharge voltage, t_d - ignition delay time, T_{off} -pulse off time) (peak current 18 A, pulse on time 400 μs, tool rotation 1500 rpm).

Table 14. Model validation.

Run order	W/p & tool	Machining parameters			MRR (mg/min)		TWR (mg/min)		SR (microns)	
		Pc (A)	Ton (μ s)	Trpm (rpm)	Experiment	Predicted, Residual, % Error	Experiment	Predicted, Residual, % Error	Experiment	Predicted, Residual, % Error
18	EN31&Gr	18	400	1800	545.3	542.0, 3.27, 0.60	98.5	93.61, 4.89, 4.97	11.23	11.45, -0.22, -1.99
22		24	100	1800	710.8	756.3, -45.54, -6.41	102.6	108.23, -5.63, -5.48	8.262	8.51, -0.25, -2.97
27		12	400	1500	302	317.8, -15.81, -5.24	73.1	79.03, -5.93, -8.11	11.487	11.49, 0.00, 0.00
6	EN31&Cu	24	400	1800	588.1	636.38, -48.28, -8.21	151.4	155.88, -4.48, -2.96	17.003	15.68, 1.32, 7.78
8		18	100	1800	284.45	282.84, 1.61, 0.57	170.5	158.48, 12.03, 7.05	8.23	8.14, 0.09, 1.09
11		18	400	1500	410.7	428.29, -17.59, -4.28	102.45	94.34, 8.11, 7.91	12.508	13.65, -1.14, -9.14

6. Regression model validation

A regression model validation is presented in table 14. The regression equations (1), (2), (3) and (4), (5), (6) were used to predict the results for EN31 and Gr and EN31 and Cu, respectively. The percentage error between the experiment and predicted values were within 10% which showed good approximation.

7. Surface Morphology

Figure 19 shows the surface morphology of the samples machined by conventional EDM and abrasive mixed rotary EDM (AREDM). The morphology of the samples machined by conventional EDM was specifically included to compare the results with abrasive mixed rotary EDM (AREDM). The surface images were captured through a field emission scanning electron microscope (FESEM) (Model: FEI Quanta 200 F SEM) with a working distance of 10 mm. The surface morphology results clearly showed improvements in surface with abrasive mixed rotary EDM with graphite electrode compared to conventional EDM. The conventional EDM surface shows segregated solidified spherical debris, clustered deposited debris, surface cracks and pockmarks as evident from figures 19(a, c). In figure 19 (b), re-deposited materials i.e. debris were effectively flushed away due to tool and stirrer rotation resulting in

smooth surface. Furthermore, it is also evident from figure 11(a) that energy density of the spark decreased due to expansion of plasma at a high pulse on time resulting in smooth surface. The same has also been verified from figure 18(a) that the spark cycle remained uniform with graphite electrode again contributing into smooth surface. On the contrary, tool and stirrer rotation effects on copper electrode have not contributed appreciably as the surface cracks along with segregated solidified debris are quite clear from figure 19(d). The reason for this may be attributed to the increased energy density of the spark at high pulse on time leading to rough surface (refer figure 17(b)) and the existence of ignition delay and dissimilar spark cycles (refer figure 18(b)).

8. Analysis of recast layer thickness

Recast layer occurs due to redeposited material or debris on the surface of workpiece. Figures 20(a-f) and 21(a-f) demonstrate the characteristics of recast layer while machining EN31 steel with graphite and copper electrode, respectively. A comparison with conventional EDM is also presented. It has been noticed that the graphite electrode resulted into a better surface with thin recast layer compared to the copper electrode in AREDM and conventional EDM with both electrodes. It recorded recast layer thickness of 6.12 μ m compared to 32.29 μ m and 62.25 μ m in AREDM and conventional EDM machined with copper

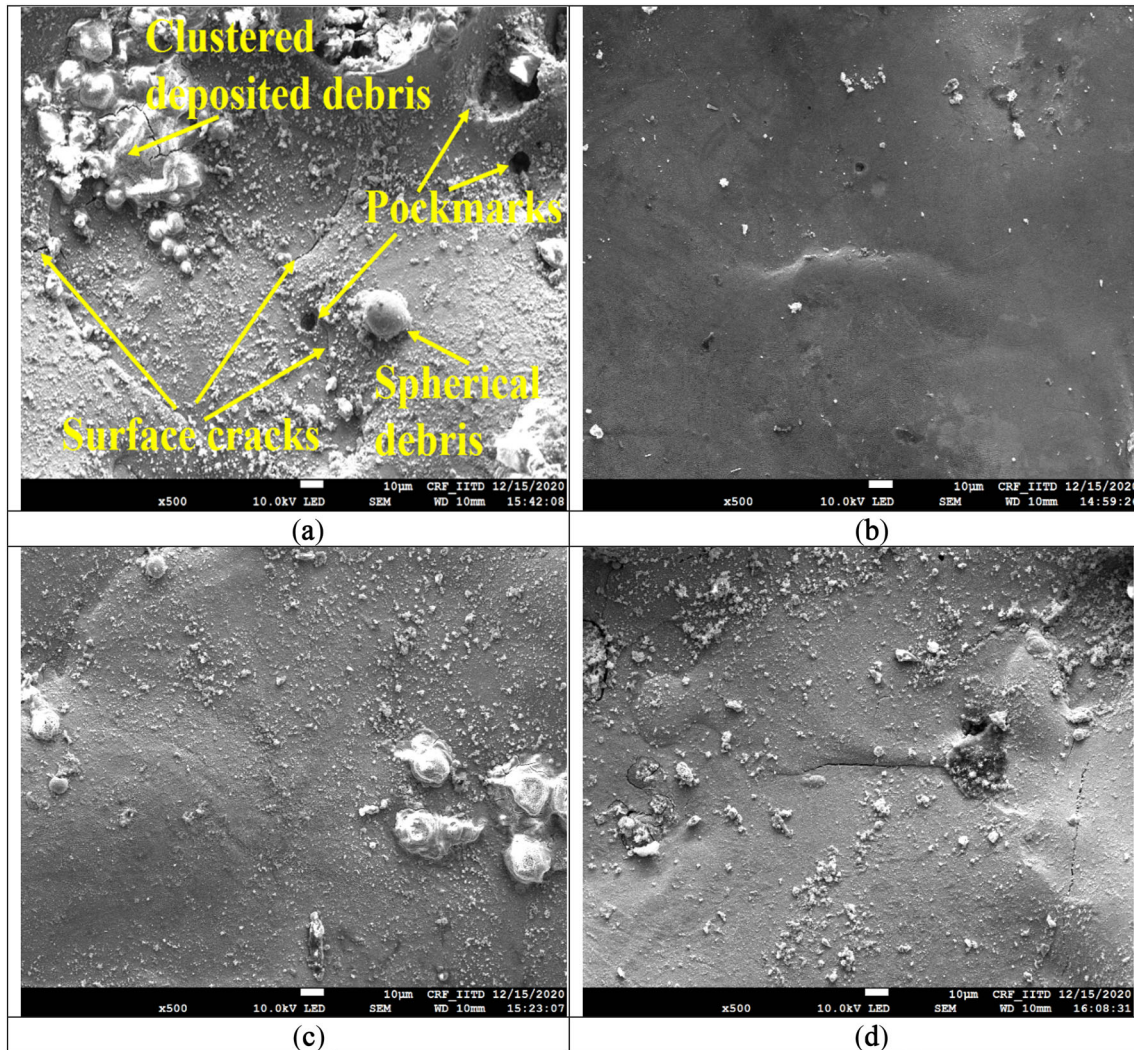


Figure 19. Morphology of surface by (a) conventional EDM (EN31 and Gr); (b) AREDM (EN31 and Gr); (c) conventional EDM (EN31 and Cu); (d) AREDM (EN31 and Cu). (peak current 18A, pulse on time 400 μ s, tool rotation 1500 rpm).

electrode, respectively (refer figures 20(e) and 21(a, d)). Micro-cracks on the surface of recast layer were seen with graphite electrode whereas, no micro-cracks were observed with copper electrode. These cracks develop due to rapid cooling cycle after melting due to flushing action of dielectric fluid. The intensity of micro-cracks were also found to be less with AREDM process refer figures 20(c, f). From figures 21(b, e), it can be clearly seen that the debris adhered to surface in conventional EDM are very large compared to debris in AREDM process. The formation of thin recast layer and finer surface in terms of smaller redeposited debris makes AREDM process better than the conventional one. The same can also be verified from figure 19. No such deposition of debris was noticed with the graphite electrode which is the reason why it results in better surface finish. Same may also be verified from surface roughness results as given in figure 7.

9. Analysis of sub-surface microhardness

Struers Duramin 40-M1 Vickers hardness tester of hardness scale HV0.5 was used to measure the sub-surface microhardness across the machining surface. As a preparatory requirement, workpieces were first prepared by fixing them in a die. The indenter was subjected to a 500 g load for 10 seconds of dwell time. Readings were taken on the surface in two perpendicular directions, namely along the edge of the surface and transverse to the surface with 8 indentations on each side. As a final outcome, the average values of these indentations were taken. The collected findings are portrayed in table 15. It is apparent that the AREDM enhances the surface's microhardness. The reason may be assigned to the migration of the powder material which increases the hardness. In this study, SiC powder is responsible for the increase of micro-hardness.

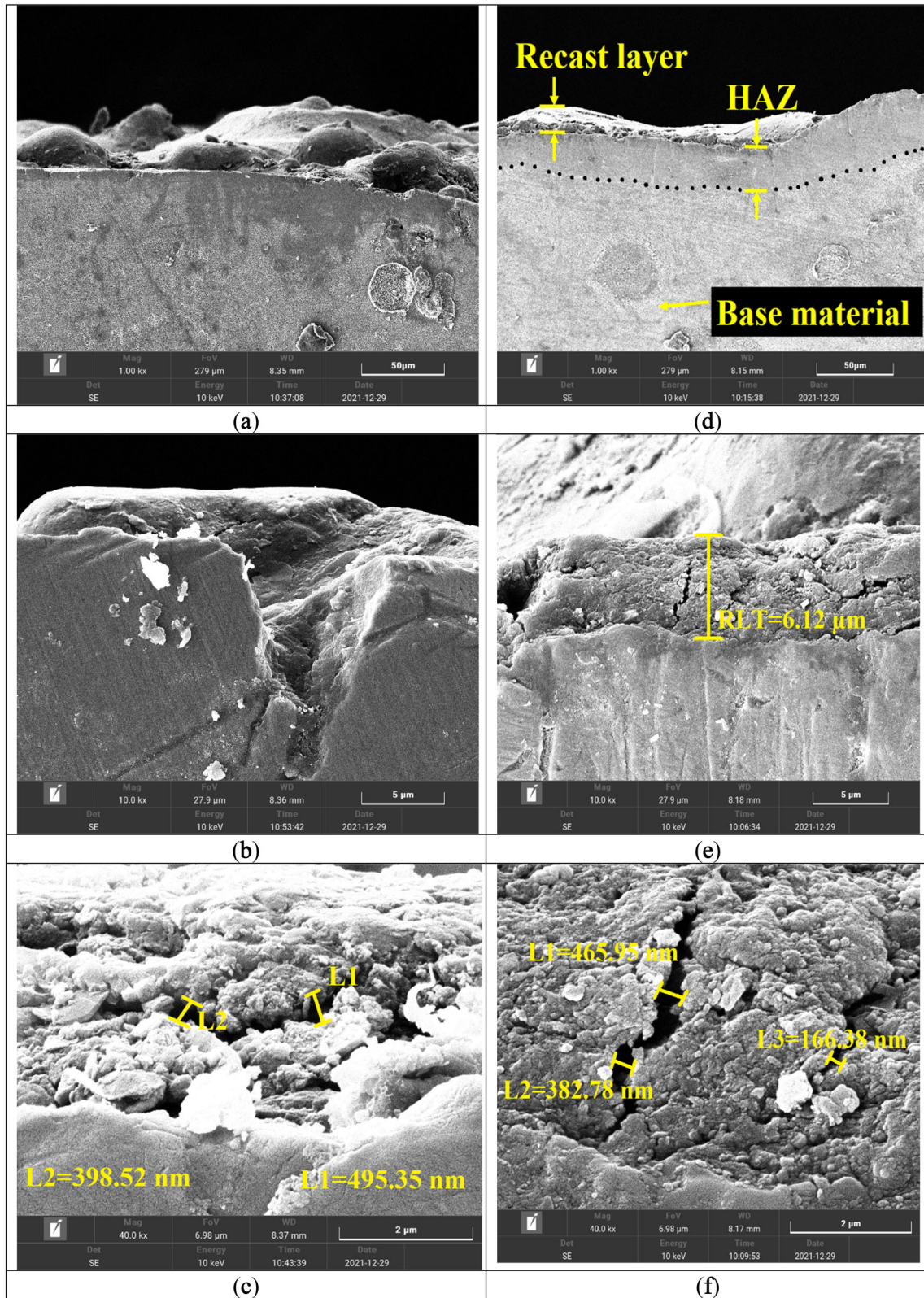


Figure 20. FESEM images of recast layer formed in (a, b, c) conventional EDM (EN31 and Gr); (d, e, f) AREDM (EN31 and Gr). (peak current 18A, pulse on time 400 μs, tool rotation 1500 rpm).

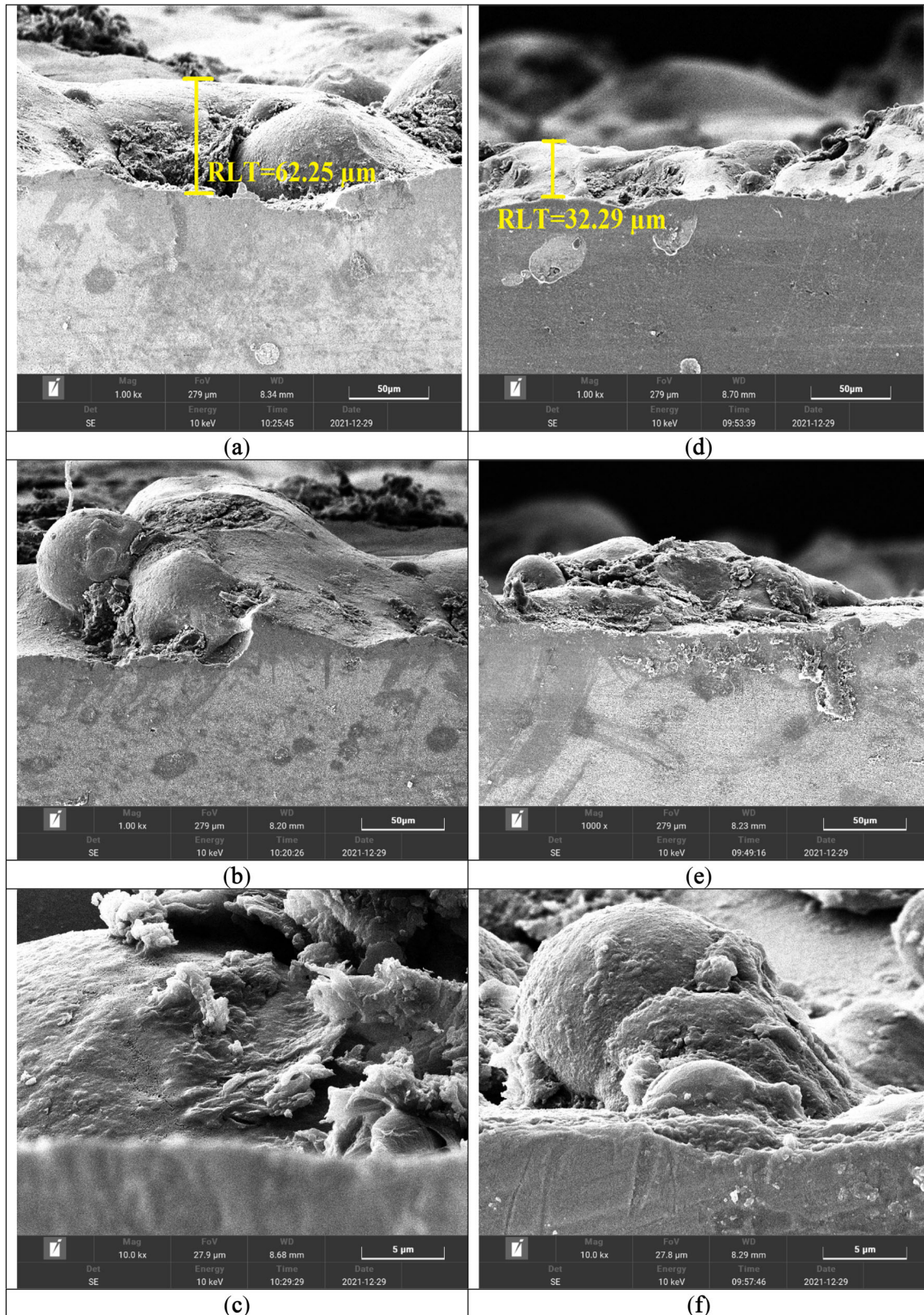


Figure 21. FESEM images of recast layer formed in (a, b, c) conventional EDM (EN31 and Cu); (d, e, f) AREDM (EN31 and Cu). (peak current 18A, pulse on time 400 μs, tool rotation 1500 rpm).

Table 15. Results of sub-surface microhardness.

Vickers hardness	Process (workpiece and tool)			
	Conventional EDM (EN31 and Gr)	AREDM (EN31 and Gr)	Conventional EDM (EN31 and Cu)	AREDM (EN31 and Cu)
Along edge	502.81	529.17	465.07	521.87
Transverse to edge	514.59	533.23	503.33	523.54

Table 16. Optimum set of process parameters.

W/p & tool	Optimum parameters			MRR (mg/min)		TWR (mg/min)		SR (microns)	
	Pc (A)	Ton (μ s)	Trpm (rpm)	Experiment	Predicted, % Error	Experiment	Predicted, % Error	Experiment	Predicted, % Error
EN31&Gr	24	100	1700	712.14	748.32, – 5.08	101.73	99.56, 2.13	8.34	8.73, – 4.67
EN31&Cu	24	100	1400	554.19	516.86, 6.73	258.6	244.39, 5.49	10.89	11.91, – 9.36

10. Multi-objective optimization

The present work involves a multi-objective optimization like in most of EDM applications. In this study, maximization of MRR along with minimization of TWR and SR, were aimed. For this purpose, genetic algorithm was selected to identify the best possible set of parameters [30]. The MATLAB (R2018a) optimization toolbox was used for executing genetic algorithm. The statistical model for MRR, TWR and SR for EN31 and Gr, represented by equations (1), (2) and (3) and for EN31 and Cu by equations (4), (5) and (6) were used in the optimization. The problem formulation with constraints is as follows

$$\text{Maximize } f_1 = \text{MRR}(\phi)$$

$$\text{Minimize } f_2 = \text{TWR}(\phi)$$

$$\text{Minimize } f_3 = \text{SR}(\phi)$$

where; $\phi = \{Pc, Ton, Trpm\}$ subjected to
 $12 \leq Pc \leq 24$; $100 \leq Ton \leq 1000$; $1200 \leq Trpm \leq 1800$

The optimum set of process parameters as revealed by the genetic algorithm multi-objective optimization technique are shown in table 16.

11. Comparison of present work with previous research

A comparison of the present research work with prior research is shown in table 17. The prior research, as per table 17, shows a mix blend of the effect of tool rotation on machining responses MRR, TWR and SR in powder mixed rotary EDM process.

12. Conclusions

The present work focused on machining of EN31 steel with two electrode material combinations i.e. graphite and the copper in abrasive mixed rotary tool EDM. The following conclusions may be drawn in machining of hardened EN31 steel (52 HRC) from the current work :

1. MRR increased with increase in peak current for both graphite as well as copper electrode. On comparing, graphite recorded more material removal and resulted into better surface finish. On the contrary, copper resulted in a rougher surface.
2. At higher peak current and pulse on time, arcing was noticed while conducting experiments with a visible dark black circle on the copper electrode. Hence, copper electrode went more erratic cycling than graphite.
3. While machining with graphite electrode, surface finish improved from 11.842 μ m to 11.23 μ m. On the contrary, with copper electrode, it increased from 12.917 μ m to 14.58 μ m.
4. Statistical modelling of the machining environment encompassing the peak current, pulse on time and tool rotation were successfully studied and verified experimentally.
5. FESEM images clearly showed the improvement on the workpiece surface with AREDM compared to conventional EDM.
6. In EN31 and Gr, the MRR was governed by pulse on time and peak current with percentage share of 57.41% and 17.63% respectively. The TWR was governed by pulse on time and tool rotation with percentage share of 40.59% and 35.85% respectively. The SR was governed by pulse on time and tool rotation with percentage share of 20.83% and 7.1% respectively.

Table 17. Comparative study with prior research.

EDM variant	W/p	Tool	Powder	Presented comparison with conventional EDM	MRR	TWR	SR	Reference
REDM	AISI D3 tool steel	Copper	—	Yes	—	—	→	[12]
PMEDM	Super Co 605	Graphite	Graphite	No	—	—	→	[17]
PMEDM	Inconel 825 superalloy	Copper	Alumina	Yes	↑	→	→	[18]
PMEDM + REDM	45 carbon steel, W18Cr4V high speed steel	Brass, copper	Silicon powder with air and liquid (Three phase mixture)	No	↓	—	—	[31]
REDM	Al-SiC MMCs	Brass, copper	—	No	↑	→	→	[32]
PMEDM + REDM	Die steel D2	Copper	Aluminium	No	MRR _{Br} > MRR _{Cu}	—	—	[33]
PMEDM + REDM	EN31 steel	Copper	MWCNT	Yes	↑	—	→	[34]
PMEDM + REDM	EN31 steel	Graphite	SiC	Yes	NA	↑	→	Present work
PMEDM + REDM	EN31 steel	Copper	SiC	Yes	↓	↑	→	Present work

HCHCr: high chromium die steel; MMCs: metal matrix composites; MWCNT: multi-wall carbon nanotube; SiC: silicon carbide; PMEDM: powder mixed EDM; REDM: rotary EDM; NA: response not affected

- In EN31 and Cu, the MRR was governed by peak current and tool rotation with percentage share of 55.86% and 13.44% respectively. The TWR was governed by pulse on time and peak current with percentage share of 44.12% and 32.59% respectively. The SR was governed by pulse on time and peak current with percentage share of 35.77% and 25.87% respectively.
- Genetic algorithm method was used for multi objective optimization. The optimum process parameter setting in the machining of EN31 and Gr (peak current 24 A, pulse on time 100 μs, tool rotation 1700 rpm) was found to yield MRR, TWR and SR to be 712.14 mg/min, 101.73 mg/min and 8.34 μm, respectively. Similarly, optimum process parameter setting in the machining of EN31 and Cu (peak current 24 A, pulse on time 100 μs, tool rotation 1400 rpm) was found to yield MRR, TWR and SR to be 554.19 mg/min, 258.6 mg/min and 10.89 μm, respectively.
- A thin recast layer thickness of 32.29 μm was formed in AREDM compared to 62.25 μm in conventional EDM when machined with the copper electrode. Comparing RLT in AREDM with graphite and copper, graphite outperformed copper tool with RLT of 6.12 μm. The graphite tool may be given preference to copper when looking for RLT.
- AREDM resulted in the enhanced sub-surface microhardness in machining EN31 steel with both graphite and copper electrodes compared with conventional EDM. This increase was noticed over the edge as well as in transverse direction.
- The results of sub-surface microhardness revealed surface modification as one of the important aspects of the abrasive mixed rotary EDM.

Acknowledgements

Authors are thankful for the laboratory support provided by Delhi Technological University, Delhi and IIT, Delhi. Funding No funding was received for carrying out this research work.

Abbreviations

- EDM Electrical discharge machining
- AREDM Abrasive rotary electrical discharge machining
- MRR Material removal rate
- TWR Tool wear rate
- SR Surface roughness
- ANOVA Analysis of variance
- Pc Peak current (ampere)
- Ton Pulse on time (micro-second)
- Trpm Tool rotation (rpm)
- Gr Graphite
- Cu Copper
- RLT Recast layer thickness

References

- [1] Lin Y C, Chen Y F, Wang D A and Lee H S 2009 Optimization of machining parameters in magnetic force assisted EDM based on Taguchi method. *J. Mater. Process. Technol.* 209: 3374–3383
- [2] Ho K H and Newman S T 2003 State of the art electrical discharge machining (EDM). *Int. J. Mach. Tools Manuf.* 43: 1287–1300
- [3] Bhattacharya A, Batish A, Singh G and Singla V K 2012 Optimal parameter settings for rough and finish machining of die steels in powder-mixed EDM. *Int. J. Adv. Manuf. Technol.* 61: 537–548
- [4] Srivastava V and Pandey P M 2013 Experimental investigation on electrical discharge machining process with ultrasonic-assisted cryogenically cooled electrode. *Proc. Inst. Mech. Eng. Part B J. Eng. Manuf.* 227: 301–314
- [5] Singh Bains P, Sidhu S S and Payal H S 2018 Investigation of magnetic field-assisted EDM of composites. *Mater. Manuf. Process.* 33: 670–675
- [6] Tao J, Shih A J and Ni J 2008 Experimental study of the dry and near-dry electrical discharge milling processes. *J. Manuf. Sci. Eng. Trans. ASME.* 130: 0110021–0110029
- [7] Singh G, Satsangi P S and Prajapati D R 2020 Effect of Rotating Magnetic Field and Ultrasonic Vibration on Micro-EDM Process. *Arab. J. Sci. Eng.* 45: 1059–1070
- [8] Aliakbari E and Baseri H 2012 Optimization of machining parameters in rotary EDM process by using the Taguchi method. *Int. J. Adv. Manuf. Technol.* 62: 1041–1053
- [9] Chow H M, Yan B H and Huang F Y 1999 Micro slit machining using electro-discharge machining with a modified rotary disk electrode (RDE). *J. Mater. Process. Technol.* 91: 161–166
- [10] Wang C C and Yan B H 2000 Blind-hole drilling of Al₂O₃/6061Al composite using rotary electro-discharge machining. *J. Mater. Process. Technol.* 102: 90–102
- [11] Satsangi P S and Chattopadhyay K D 2010 A study of machining parameters during electrical discharge machining of steel by a rotary copper electrode. *Adv. Mater. Res.* 83–86: 756–763
- [12] Dwivedi A P and Choudhury S K 2016 Improvement in the Surface Integrity of AISI D3 Tool Steel Using Rotary Tool Electric Discharge Machining Process. *Procedia Technol.* 23: 280–287
- [13] Chattopadhyay K D, Verma S, Satsangi P S and Sharma P C 2009 Development of empirical model for different process parameters during rotary electrical discharge machining of copper-steel (EN-8) system. *J. Mater. Process. Technol.* 209: 1454–1465
- [14] Singh N K, Pandey P M and Singh K K 2017 Experimental investigations into the performance of EDM using argon gas-assisted perforated electrodes. *Mater. Manuf. Process.* 32: 940–951
- [15] Kansal H K, Singh S and Kumar P 2005 Parametric optimization of powder mixed electrical discharge machining by response surface methodology. *J. Mater. Process. Technol.* 169: 427–436
- [16] Kansal H K, Singh S and Kumar P 2007 Effect of silicon powder mixed EDM on machining rate of AISI D2 die steel. *J. Manuf. Process.* 9: 13–22
- [17] Singh A K, Kumar S and Singh V P 2015 Effect of the addition of conductive powder in dielectric on the surface properties of superalloy Super Co 605 by EDM process. *Int. J. Adv. Manuf. Technol.* 77: 99–106
- [18] Kumar A, Mandal A, Dixit A R, Das A K, Kumar S and Ranjan R 2019 Comparison in the performance of EDM and NPMEDM using Al₂O₃ nanopowder as an impurity in DI water dielectric. *Int. J. Adv. Manuf. Technol.* 100: 1327–1339
- [19] Joshi A Y and Joshi A Y 2019 A systematic review on powder mixed electrical discharge machining. *Heliyon.* 5: e02963
- [20] Bhattacharya A, Batish A and Kumar N 2013 Surface characterization and material migration during surface modification of die steels with silicon, graphite and tungsten powder in EDM process. *J. Mech. Sci. Technol.* 27: 133–140
- [21] Surani K 2020 Effect on Powder Mixed Electric Discharge Machining (PMEDM) on Various Materials with Different Powders: A Review. *Int. J. Res. Appl. Sci. Eng. Technol.* 8 (12): 614–630
- [22] Che Haron C H, Ghani J A, Burhanuddin Y, Seong Y K and Swee C Y 2008 Copper and graphite electrodes performance in electrical-discharge machining of XW42 tool steel. *J. Mater. Process. Technol.* 201: 570–573
- [23] Torres A, Puertas I and Luis C J 2015 Modelling of surface finish, electrode wear and material removal rate in electrical discharge machining of hard-to-machine alloys. *Precis. Eng.* 40: 33–45
- [24] Dhar S, Purohit R, Saini N, Sharma A and Kumar G H 2007 Mathematical modeling of electric discharge machining of cast Al-4Cu-6Si alloy-10 wt.% SiCP composites. *J. Mater. Process. Technol.* 194: 24–29
- [25] Expo Tools Pvt. Ltd., "<https://expomachinetools.com/>, September 17, 2021
- [26] Young H D 1992 *University Physics*, Addison-Wesley Pub. Co
- [27] Thought Co. <https://www.thoughtco.com/table-of-electrical-resistivity-conductivity-608499> Accessed on 2021 May 17
- [28] Chow H M, Yang L D, Lin C T and Chen Y F 2008 The use of SiC powder in water as dielectric for micro-slit EDM machining. *J. Mater. Process. Technol.* 195: 160–170
- [29] Beravala H and Pandey P M 2018 Experimental investigations to evaluate the effect of magnetic field on the performance of air and argon gas assisted EDM processes. *J. Manuf. Process.* 34: 356–373
- [30] Konak A, Coit D W and Smith A E 2006 Multi-objective optimization using genetic algorithms: A tutorial. *Reliab. Eng. Syst. Saf.* 91: 992–1007
- [31] Bai X, Zhang Q, Zhang J, Kong D and Yang T 2013 Machining efficiency of powder mixed near dry electrical discharge machining based on different material combinations of tool electrode and workpiece electrode. *J. Manuf. Process.* 15: 474–482
- [32] Mohan B, Rajadurai A and Satyanarayana K G 2002 Effect of SiC and rotation of electrode on electric discharge machining of Al-SiC composite. *J. Mater. Process. Technol.* 124: 297–304
- [33] Gurule N B and Nandurkar K N 2012 Effect of Tool Rotation on Material Removal Rate during Powder Mixed Electric Discharge Machining of Die Steel. *Int. J. Emerg. Technol. Adv. Eng.* 2: 328–332
- [34] Bajaj R, Dixit A R, Tiwari A K and Chauhan N K 2020 Machining performance enhancement of en-31 diesteel using mwent mixed rotary edm. *Indian J. Eng. Mater. Sci.* 27: 309–319